Zuerst erschienen in: Solid State Ionics 118 (1999) 43-66

Ionic thermopower of composite electrolytes
I. Theory

M. Vennekamp, J. Janek*

Institut für Physikalische Chemie und Elektrochemie Universität Hannover, Callinstr. 3-3A, 30167 Hannover, Germany

Abstract

The ionic thermopower of solid electrolyte composites which are composed of a solid electrolyte and an electrically insulating inert phase is analyzed. For a stoichiometric model system AX with Frenkel disorder in the cation sublattice we derive formal relations within a lattice point defect model for the change in ionic thermopower on dispersing the second phase. It is shown that thermopower measurements may provide information on the defect concentrations in the space charge regions surrounding the inert phase. Available experimental results are discussed.

Keywords: Thermopower; Solid electrolytes; Ionic conduction; Interfaces; Space charges

1. Introduction

Since the first experiments by Liang [1] on LiI:Al_2O_3 composites numerous studies have been performed on various solid electrolyte composites. Major theoretical and experimental work has been reported by Maier et al. [2], cf. also [3,4]. Applying a solution of the Poisson-Boltzmann equation as obtained originally by Frenkel, Lehovec and Kliewer [5–8], Maier analyzes the conductivity of solid electrolyte composites on the basis of a space charge model. He assumes an attractive interaction between mobile charged defects and the surface of the dispersed inert phase, leading to a space charge region with defect concentrations differing from the intrinsic bulk concentrations. With decreasing temperature, i.e. with decreasing intrinsic defect concentrations and increasing Debye length, the (positive or negative) relative excess conductivity due to the space charge regions increases. Maier performed extensive experimental studies on the model systems AgBr:Al_2O_3 and AgCl:Al_2O_3 and concluded that adsorption of silver cations at the Al_2O_3 surface leads to a positive excess conductivity of the space charge region due to an increased vacancy concentration [2].

In addition to conductivity measurements which provide combined information on both charge carrier concentrations c_j and mobilities u_j, thermopower measurements provide further information primarily on charge carrier concentrations (e.g. [9]). The combined application of both conductivity and thermopower measurements allows far-reaching conclusions on the defect structure of electrically conducting materials [10]. A well known example is repre-

*Corresponding author. E-mail: janek@mbox.pci.uni-hannover.de

sented by the cation conductor AgBr (AgCl) homogeneously doped with $CdBr_2$ ($CdCl_2$) [11]. Both the change in the ionic conductivity and thermopower can be understood quantitatively on the basis of a simple lattice point defect model [12,13]. Equivalent examples are provided by studies of electronic defects in pure and doped semiconductors.

Our formal treatment of the ionic thermopower of composite electrolytes in Section 2 is based on the analysis of the thermopower of inhomogeneously doped conductors as model systems for space charge layers. In the following we present a formal solution for different limiting cases, starting with the thermopower of simple bicrystals. In any case, a comparison of the thermopower of pure and (either homogeneously or inhomogeneously) doped crystals provides at least qualitative information on the differences in defect concentration.

The thermopower of electrolyte composites which are frequently regarded as ''heterogeneously'' doped crystals has yet not been studied systematically. A study of Shahi and Wagner on $AgI:Al_2O_3$ composites [14] provides the only available experimental data on the ionic thermopower of electrolyte composites to our knowledge. Their major results are discussed together with our own preliminary experimental results on the basis of our formal analysis in Section 3. To date, conductivity measurements still provide the major experimental evidence for an increased defect concentration in space charge regions.

Finally, the information content of thermopower measurements on composites is discussed in a more general sense in Section 4. An inherent problem in the quantitative analysis of thermopower data is the magnitude of the so-called heats of transport and the entropies of the individual point defects (structure elements). The heats of transport are neither known from theory nor are they accessible by experiments. Furthermore, it is questionable whether the heat of transport or the entropy contribution of a lattice defect is changed by the presence of a second phase with different thermal and mechanical properties.

2. Formal treatment

Our formal treatment is organized as follows: We start in Section 2.1 and Section 2.2 with a brief review of the basic relations for the description of ionic thermocells and the necessary formal relations describing the thermopower of pure and (homogeneously) doped ionic conductors in terms of lattice point defects. $CdCl_2$-doped AgCl is discussed as a model system. The essential relations from the studies on space charges by Kliewer [8] and on ionic conduction in space charges by Maier [2] in Section 2.3 complete the introductory part. Thereafter we regard two basic experimental arrangements of asymmetric bicrystals composed of a pure and a doped crystal with their interface being oriented either parallel or perpendicular to the temperature gradient (Section 2.4). It follows the analysis of two more complicated cases in Section 2.5 and Section 2.6, viz, an inhomogeneously doped crystal with a concentration gradient (given by the concentration gradient of defects in a space charge layer) parallel or perpendicular to the temperature gradient. Finally, we discuss the thermopower of a composite regarding a simple brick layer arrangement of the two phases (Section 2.7).

2.1. Thermogalvanic cells

Historically, two major and equivalent concepts for the description of thermogalvanic cells exist. In the context of solid state physics, the thermovoltage U of a thermogalvanic cell is often represented as the sum of two contributions to the overall electric potential difference: (a) the homogeneous (U_{hom}) and (b) the heterogeneous thermovoltage (U_{het}) (cf. [13]). The so-called homogeneous thermovoltage corresponds to the electric potential difference which is created within a single nonisothermal phase. The so-called heterogeneous thermovoltage corresponds to the potential drops at the interfaces of the thermogalvanic cell.

In a physicochemical approach to thermogalvanic cells involving mixed conducting solids, Wagner [15] introduced a description in terms of electrochemical potentials $\tilde{\mu}_i$. This description has the advantage of a straightforward presentation within the framework of irreversible thermodynamics, using potentials which are directly accessible via experiments. For the sake of consistency with the paper of Wagner on thermogalvanic cells we will use his notation throughout.

The measurable emf U of the thermogalvanic cell in Fig. 1 as the difference of the galvanic potentials

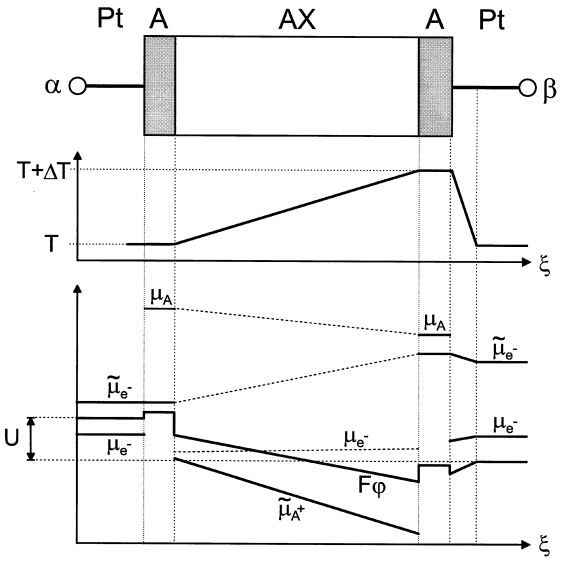

Fig. 1. Galvanic cell for the measurement of the ionic thermopower of a binary crystal AX with negligible electronic conductivity: Pt(α,T)|A(T)|AX(T)|AX($T+\Delta T$)|A($T+\Delta$T)|Pt(β,$T+\Delta T$)|Pt(β,T).

φ in the isothermal inert and equal contacts α and β (at laboratory temperature T) can be expressed as the difference in the electrochemical potential of the electrons in the contacts:

$$U = \Delta\varphi = \varphi(\mathrm{Pt},\beta) - \varphi(\mathrm{Pt},\alpha) = -\frac{1}{F}\left[\tilde{\mu}_{e'}(\mathrm{Pt},\beta) - \tilde{\mu}_{e'}(\mathrm{Pt},\alpha)\right] \quad (1)$$

Assuming local electrochemical equilibrium at all interfaces and introducing the electrochemical potential $\tilde{\mu}_{\mathrm{A}^+}$ of cations A^+ via the equilibrium condition

$$\tilde{\mu}_{\mathrm{A}^+}(\mathrm{AX}) = \mu_{\mathrm{A}}(\mathrm{A}) - \tilde{\mu}_{e'}(\mathrm{A}) \quad (2)$$

we obtain the thermal emf as the sum of three contributions,

$$\Delta\varphi = \frac{1}{F}\left[\tilde{\mu}_{\mathrm{A}^+}(\mathrm{AX},T+\Delta T) - \tilde{\mu}_{\mathrm{A}^+}(\mathrm{AX},T)\right] - \frac{1}{F}\left[\mu_{\mathrm{A}}(\mathrm{A},T+\Delta T) - \mu_{\mathrm{A}}(\mathrm{A},T)\right] + \frac{1}{F}\left[\tilde{\mu}_{e'}(\mathrm{Pt},T+\Delta T) - \tilde{\mu}_{e'}(\mathrm{Pt},T)\right] \quad (3)$$

In differential form Eq. (3) results as

$$\mathrm{d}\varphi = \frac{1}{F}\cdot\left[\mathrm{d}\tilde{\mu}_{\mathrm{A}^+}(\mathrm{AX}) - \mathrm{d}\mu_{\mathrm{A}}(\mathrm{A}) + \mathrm{d}\tilde{\mu}_{e'}(\mathrm{Pt})\right] \quad (4)$$

Dividing Eq. (4) by the temperature difference dT, introducing the absolute ionic thermopower ϵ_{A^+} (AX) of the solid electrolyte,

$$\epsilon_{\mathrm{A}^+} = \epsilon_{\mathrm{A}^+}(\mathrm{AX}) \equiv \frac{1}{F}\left[\frac{\mathrm{d}\tilde{\mu}_{\mathrm{A}^+}(\mathrm{AX})}{\mathrm{d}T} - \frac{\mathrm{d}\mu_{\mathrm{A}}(\mathrm{A})}{\mathrm{d}T}\right] = \frac{1}{F}\left[\frac{\mathrm{d}\tilde{\mu}_{\mathrm{A}^+}(\mathrm{AX})}{\mathrm{d}T} + S_{\mathrm{A}}^{\circ}\right] \quad (5)$$

and the absolute electronic thermopower $\epsilon_{e'}$ (Pt) of platinum,

$$\epsilon_{e'}(\mathrm{Pt}) \equiv -\frac{1}{F}\cdot\frac{\mathrm{d}\tilde{\mu}_{e'}(\mathrm{Pt})}{\mathrm{d}T}, \quad (6)$$

one ends with the relation

$$\epsilon \equiv \frac{\mathrm{d}\varphi}{\mathrm{d}T} = \epsilon_{\mathrm{A}^+} - \epsilon_{e'}(\mathrm{Pt}) \quad (7)$$

which describes the operationally defined thermopower of the thermogalvanic cell in Fig. 1.

The definition of the absolute ionic thermopower according to Eq. (5) is rather an operational choice and is not unique. The ionic thermopower can only be measured by the use of reversible metal electrodes (A), and thus, the inclusion of the molar metal entropy S_{A}° into the definition appears justified. It has to be noted that in the case of mixed-conducting materials with a non-negligible electronic transference number, an auxiliary solid electrolyte has to be inserted between AX and A. This leads to an additional term in Eq. (7) representing the ionic thermopower of the auxiliary electrolyte.

Regarding Eqs. (4) and (5), the calculation of an experimental thermovoltage requires the knowledge of the electrochemical potential difference $d\tilde{\mu}_{\mathrm{A}^+}(\mathrm{AX})/\mathrm{d}T$ of the mobile ions A^+ in the electrolyte, the metal entropy S_{A}° and the thermopower of platinum $\epsilon_{e'}$(Pt). Whereas the latter two quantities are readily available from the literature, $\mathrm{d}\tilde{\mu}_{\mathrm{A}^+}(\mathrm{AX})/\mathrm{d}T$ has to be provided by suitable models of the defect thermodynamics and kinetics of AX.

In terms of the ions A^+ (not specifying any mobile defect), $\mathrm{d}\tilde{\mu}_{\mathrm{A}^+}(\mathrm{AX})$ has to be derived from the flux equation

$$j_{\mathrm{A}^+} = -L_{\mathrm{A}^+}\left[\nabla\tilde{\mu}_{\mathrm{A}^+} + \left(\bar{S}_{\mathrm{A}^+} + \frac{Q^*_{\mathrm{A}^+}}{T}\right)\cdot\nabla T\right] \quad (8)$$

which results from the combination of point defect thermodynamics and linear irreversible thermodynamics [16,17], see Appendix (A.1). In Eq. (8), L_{A^+} represents the phenomological transport coefficient of ions A^+, S_{A^+} denotes the partial entropy of ions A^+ and $Q^*_{A^+}$ denotes the (reduced) heat of transport of ions. In the stationary state the flux j_{A^+} vanishes for materials with negligible electronic conductivity and we obtain

$$\frac{\mathrm{d}\tilde{\mu}_{A^+}}{\mathrm{d}T} = -\left(\bar{S}_{A^+} + \frac{Q^*_{A^+}}{T}\right) \equiv -S^*_{A^+} \tag{9}$$

The sum of the partial entropy $\bar{S}_{A^+}$ and the heat of transport term $Q^*_{A^+}/T$ of the ions A^+ is frequently called ''*entropy of transport*'' which is clearly a misleading expression. However, $S^*_{A^+}$ as an abbreviation simply shortens many expressions, and therefore we will use it in the following. Combining Eqs. (5) and (9), the ionic thermopower of AX can be written as:

$$\epsilon_{A^+} = -\frac{1}{F}(S^*_{A^+} - S^\circ_A) \tag{10}$$

2.2. The homogeneous systems AX *and* $A_1 - 2yB_yX$

We consider a binary (cubic) crystal AX ($z_A = 1$) with Frenkel disorder in the cation sublattice (Kröger-Vink-notation),

$$A^\times_A + V^\times_i \rightleftharpoons A^\bullet_i + V'_A \quad K_F = \exp(-\Delta G^\circ_F/kT) \tag{11}$$

The pure crystal contains equal (intrinsic) concentrations of interstitials and vacancies ($c^\#_i = c^\#_v$)[1] which depend only on temperature and pressure. Doping AX with BX_2 ($z_B = 2$) the divalent cations B^{2+} occupy regular cation sites,

$$BX_2 = B^\bullet_A + V'_A + 2X^\times_X \tag{12}$$

and the molar concentration c_v of vacancies is increased. Correspondingly, the concentration c_i of interstitials is decreased. The degree of doping can be expressed favorably by the normalized concentrations α_i or α_v,

$$\alpha_i \equiv \frac{c_i}{c^\#_i} \quad \alpha_v \equiv \frac{c_v}{c^\#_v} \qquad \alpha_i \cdot \alpha_v = 1 \tag{13}$$

which become unity for the pure crystal.

The ionic conductivity σ_{A^+} depends on both the concentrations c_i and c_v and the (electrochemical) mobilities u_i and u_v of interstitials $A^\bullet_i$ and vacancies $V^\times_i$:

$$\sigma_{A^+} = F^2 \cdot L_{A^+} \tag{14}$$

$$= F \cdot \frac{\sqrt{K_F}}{V_m} \cdot (u_i\alpha_i + u_v\alpha_i^{-1}) \tag{15}$$

Introducing the mobility ratio $\psi_i \equiv u_i/u_v$, the conductivity ratio $\sigma_{A^+}/\sigma^\#_{A^+}$ can be expressed as:

$$\frac{\sigma_{A^+}}{\sigma^\#_{A^+}} = \frac{\psi_i\alpha_i^2 + 1}{\psi_i + 1} \tag{16}$$

As shown in Fig. 2, σ_{A^+} shows a minimum at $\alpha_i(\sigma_{min}) = \psi_i^{1/2}$. The slopes $\partial \ln \sigma_{A^+}/\partial \ln \alpha_i$ equal $+1$ in the interstitial-type region and -1 in the vacancy-type region. In the case of the silver halides as our model systems the interstitials generally exhibit a higher mobility than the vacancies ($\psi_i > 1$), and thus, the conductivity minimum is shifted toward the vacancy-type region ($\alpha_i < 1$) [18]. The temperature dependence of the ionic conductivity of the pure crystal AX is determined by both the Frenkel enthalpy ΔH°_F and the migration enthalpies $\Delta H_{m,def}$

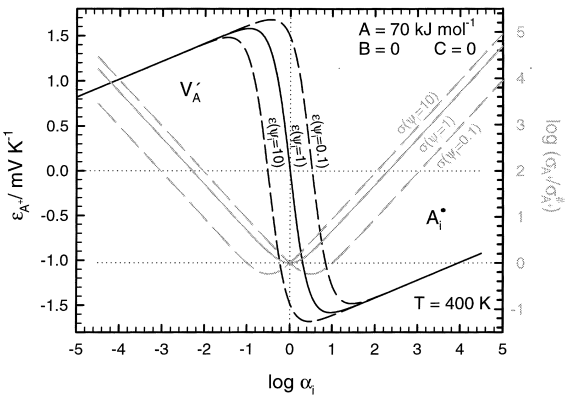

Fig. 2. Normalized ionic conductivity $\sigma_{A^+}/\sigma^\#_{A^+}$ and ionic thermopower ϵ_{A^+} of a crystal AX with cation Frenkel disorder as a function of the normalized interstitial concentration α_i (cf. Eqs. (16) and (17)) for different mobility ratios ψ_i.

[1] In the following the subscript # denotes properties of the pure crystal AX (intrinsic defect concentration).

of the defects. If the mobilities of both defects differ sufficiently, the activation energy $E_{a,\sigma}$ can be approximated as $E_{a,\sigma} \simeq \Delta H_{m,def} + 1/2\Delta H_F^\circ$, with $\Delta H_{m,def}$ being the migration enthalpy of the more mobile defect.

The ionic thermopower ϵ_{A^+} in the steady state $(j_{A^+} = 0)$[2] can be expressed on the basis of Eq. (5) as:

$$\epsilon_{A^+} = -\frac{1}{F}\left(\frac{A}{T}\cdot \tanh \ln \psi_i^{1/2}\alpha_i - R \ln \alpha_i + \frac{B}{T} + C - S_A^\circ\right) \quad (17)$$

with the abbreviations

$$A \equiv \frac{Q_i^* + Q_v^* + \Delta H_F^\circ}{2}, \quad B \equiv \frac{Q_i^* - Q_v^*}{2}$$

$$\text{and} \quad C \equiv \frac{S_i^\circ - S_v^\circ}{2} \quad (18)$$

and includes a number of additional defect parameters: S_i° and S_v° represent the standard entropies of interstitials and vacancies, respectively. The heats of transport, Q_i^* and Q_v^*, represent the heat which is transferred by an isothermal flux of interstitials and vacancies, respectively. Eq. (17) was derived earlier independently by Howard and Lidiard [13] and by Haga [20]. A derivation of the corresponding relation for the electronic thermopower on the basis of thermodynamic arguments has been given by Wagner [15] and other authors [21–24]. A straightforward derivation in the framework of linear irreversible thermodynamics and point defect thermodynamics is described by Korte and Janek [25,26]. A short summary of this derivation can be found in Appendix (A.1).

Like σ_{A^+}, ϵ_{A^+} also exhibits a characteristic dependence on α_i, see Fig. 2. The thermopower shows a s-curved shape with an inflexion point at $\alpha_{i,IP} = \psi_i^{-1/2}$, i.e. the inflexion point is shifted toward the v-type region for $\psi_i > 1$, and the thermopower at $\alpha_i = 1$ depends on ψ_i. The values of Q_i^* Q_v^*, S_i° and S_v° lead to a shift of the thermopower curve in vertical direction and also influence the thermopower at $\alpha_i = 1$. The slope of ϵ_{A^+} vs. log α_i equals $2.3R/F \simeq +200\mu V/K$ for both small and large values of α_i. The thermopower difference between its two extrema equals approximately $(Q_i^* + Q_v^* + \Delta H_F^\circ)/FT$ and the slope of the $\epsilon_{A^+} - \alpha_i$ curve in the inflexion point can be approximated as $-(Q_i^* + Q_v^* + \Delta H_F^\circ - RT)/FT$.

Regarding Fig. 2 and summarizing, it is important to realize that a simple conclusion on whether v- or i-type conductivity prevails cannot be drawn from the sign of the thermopower for nearly intrinsic material. Close to and within the intrinsic defect regime ($\alpha_i \approx 1$) the thermopower is strongly influenced by the mobility ratio ψ_i.

For materials with either predominantly interstitial ($c_v \to 0$; $\epsilon_{A^+}(i)$) or vacancy-type ($c_i \to 0$; $\epsilon_{A^+}(v)$) defects, Eq. (17) simplifies to

$$\epsilon_{A^+}(i) = -\frac{1}{F}\left(S_i^\circ - R \ln c_i + \frac{Q_i^*}{T} - S_A^\circ\right) \quad (19)$$

or

$$\epsilon_{A^+}(v) = \frac{1}{F}\left(S_v^\circ - R \ln c_v + \frac{Q_v^*}{T} + S_A^\circ\right), \quad (20)$$

respectively, and becomes independent of ψ_i. Both equations are widely used in the interpretation of thermopower data of strongly doped materials. They relate an easily measurable quantity directly to a defect concentration, being independent from the corresponding defect mobility (cf. the mobility independent linear thermopower dependence in the extrinsic regimes in Fig. 2).

The measured temperature dependence of the thermopower of pure and (homogeneously) $CdCl_2$-doped AgCl crystals is depicted as an example in Fig. 3. For pure material ($\alpha_i = 1$) Eq. (17) simplifies to

$$\epsilon_{A^+}^{\#} = -\frac{1}{F}\left(\frac{A}{T}\cdot\frac{\psi_i - 1}{\psi_i + 1} + \frac{B}{T} + C + S_A^\circ\right) \quad (21)$$

which in a first approximation always shows a simple hyperbolic temperature dependence. Vacancy doped material exhibits a characteristic s-shaped curve with a maximum that strongly depends on the degree of doping. Since the applied temperature differences are only of the order of a few Kelvin, i.e. $\Delta T/T < 1\%$, the temperature dependence of ϵ is usually neglected in a thermopower experiment.

[2]Compounds with a finite range of homogeneity generally are subject to thermal diffusion i.e. a partial demixing (Soret effect) will take place. This change of the local composition leads to a variation of the measurable thermopower with time, cf. [19].

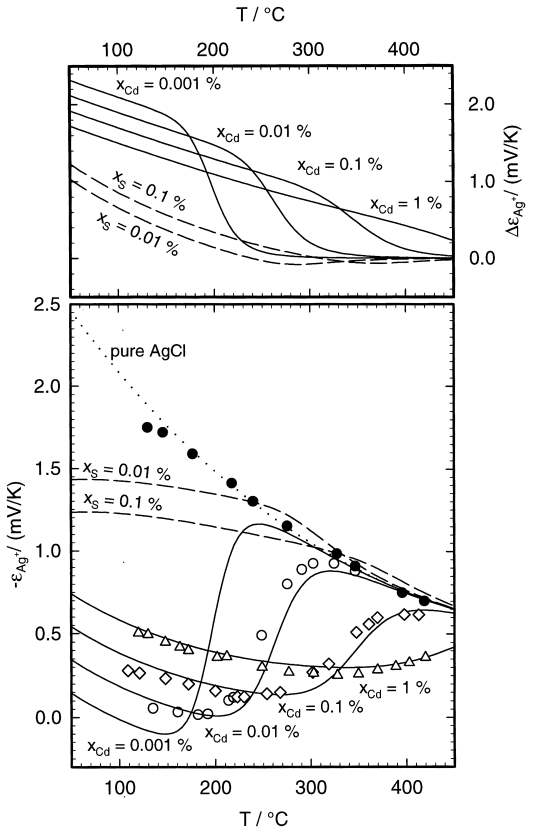

Fig. 3. The temperature dependence of the ionic thermopower of pure and $CdCl_2$-doped AgCl; experimental data by Christy [11] are represented by symbols, lines represent data calculated by use of Eq. (17) with the necessary parameters also taken from [11].

Christy fitted Eq. (17) to his experimental data and thus obtained the parameters A, B and C as functions of temperature, using mobility data of Teltow [18]. The resulting curves (solid lines) describe the experimental results quite satisfactorily. In Section 2.7, we will use Christy's values for A, B and C also for the calculation of the thermopower of AgCl:Al_2O_3 dispersions. The validity of this parameter transfer is discussed in Section 4.

Finally it should be noted that the whole formalism, which is here applied to ionic crystals with Frenkel disorder, also applies to Boltzmann-type semiconductors. Correspondingly, Eqs. (16) and (17), as our final results, can also be used for the description of the electronic thermopower in Boltzmann-type semiconductors, cf. [21–23].

2.3. The space charge model of composite electrolytes

Surfaces and interfaces of liquid and solid electrolytes generally possess excess charges which are compensated by a diffuse space charge region of counter-charged species. The electric potential and the charge distribution in the space charge region are related by the Poisson-Boltzmann differential equation. An exact solution to this equation is not possible in cylindrical or spherical geometry but approximate solutions have been reported by different authors. The Poisson-Boltzmann equation for the case of the free surface of an ionic crystal containing charged point defects was first treated by Frenkel [5]. A more elaborate treatment which has been used by Maier in his model of space charge conduction in solid electrolyte composites is reported by Kliewer [8]. For low defect concentrations, i.e. at sufficiently large Debye lengths, the defect concentrations in a space charge region can be calculated on the basis of Kliewer's solution, by assuming that the underlying defect thermodynamics and the crystal structure are identical for the crystal bulk and the space charge region.

Ready-to-use relations for an isothermal 1:1 stoichiometric crystal AX with Frenkel disorder in the terms of the normalized defect concentrations α_i and α_v can be found in [2]:

$$\alpha_v(\xi) = \frac{[1 - \vartheta_v \cdot \exp(-\xi)]^2}{[1 - \vartheta_v \cdot \exp(-\xi)]^2} = \alpha_i^{-1}(\xi). \qquad (22)$$

ξ is the normalized space variable perpendicular to the interface according to Fig. 4 and is defined as

$$\xi \equiv \frac{x}{\lambda_D} \qquad \lambda_D \equiv \left(\frac{\epsilon_0 \epsilon_r kT}{e_0^2 N_A} \cdot \frac{V_m}{2\sqrt{K_F}} \right)^{1/2}, \qquad (23)$$

where λ_D represents the Debye length. ϑ_v is a parameter describing the magnitude of the boundary effect. It varies between 0 and $+1$ for an enrichment and between 0 and -1 for a depletion of vacancies in the space charge layer. It is related to the normalized concentrations $\alpha_{i,0}$ or $\alpha_{v,0}$ of interstitials or vacancies in the first crystal layer next to the interface, respectively, and is defined as

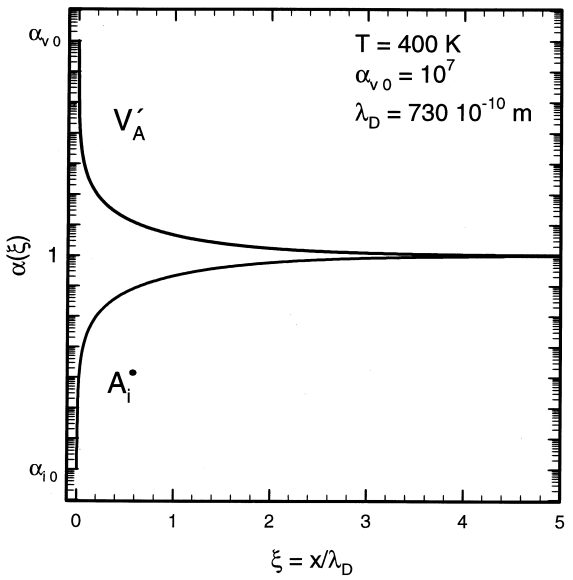

Fig. 4. Theoretical concentration profiles of interstitials and vacancies in a space charge layer of AgCl according to Eq. (22). The surface interaction parameter $\alpha_{v,o}$ is taken from Maier [2].

$$\vartheta_v = \frac{\sqrt{\alpha_{v,0}} - 1}{\sqrt{\alpha_{v,0}} + 1} = -\vartheta_i. \tag{24}$$

The excess conductivity of a heterogeneously doped crystal has been calculated by Maier on the basis of the theoretical concentration profile $\alpha_v(\xi)$ in a space charge region. Only plane boundaries parallel and perpendicular to the electric current are usually considered for the sake of simplicity ''brick layer model''. A theoretical concentration profile for a typical model system in a space charge layer calculated with Eq. (22) is depicted in Fig. 4. As shown in Appendix (A.2), the concentration function $\alpha_i(\xi)$ (and $\alpha_v(\xi)$) is virtually undisturbed by a small temperature difference in the direction of ξ. Thus, we can safely use $\alpha_i(\xi)$ for the evaluation of the thermopower of space charge regions. To take the temperature dependence of the adsorption equilibrium into account, we apply the function

$$\alpha_{v,0} = \exp\left(-\frac{\Delta_v G^\circ_{SA}}{RT}\right) / \exp\left(-\frac{\Delta G^\circ_F}{2RT}\right) \tag{25}$$

to our calculations in Section 2.7. $\Delta_v G^\circ_{SA}$ represents the free enthalpy which accounts for the specific adsorption of silver interstitials at the halide/alumina interface. Eq. (25) has been determined for $AgCl:Al_2O_3$ composites by Maier [2].

A simple physical limit of $\alpha_{v,0}$ is given by the condition that not more than a monolayer of charge carriers can adsorb on the surface of the insulator grain. Thus, the corresponding maximum charge within the space charge should be restricted to that value. Setting a maximum charge density on the surface arbitrarily as $\cong 180\mu C/\mathrm{cm}^2$ (corresponding to $e_0/9\text{Å}^2$), the integration of Eq. (22) yields a value of $\alpha_{iv,0} = 4.7\times10^9$ or $\vartheta_{iv,0} = 0.999971$ as the outer limits for $\alpha_{iv,0}$. Definitely these limits will not be approached in a real system, and thus, we restrict our calculations to $-5 < \log\ \alpha_{i,0} < 5$.

2.4. Thermopower of a bicrystal with its interface perpendicular to the temperature gradient

As may be seen from Fig. 4, a space charge region extends roughly over a length of $2\lambda_D$. In a first step, we will treat in this section a crystal with a space charge region as a ''bicrystal'', being composed of one part with intrinsic defect concentrations ($\alpha_i^I = 1$) and the other part with a different defect concentration ($\alpha_i^{II} \neq 1$). This second part can be regarded as a space charge region represented by an increased (homogeneous) mean defect concentration.

In Fig. 5 the experimental arrangement of such a ''bicrystal'' $AX(\alpha_i^I = 1)|AX(\alpha_i^{II} \neq 1)$ with its inter-

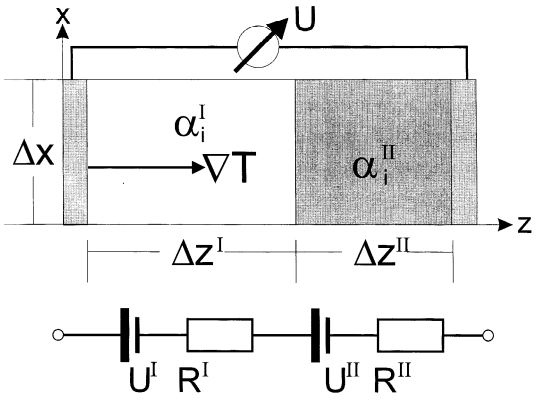

Fig. 5. A bicrystal composed of two ionic crystals AX with different defect concentrations. Region I contains no impurities (intrinsic disorder, i.e. $\alpha_i^I = 1$). Region II is homogeneously doped ($\alpha_i^{II} \neq 1$).

face perpendicular to the temperature gradient ∇T is depicted, together with its representation in terms of a simple electric circuit.

We assume that the virtual dopant in region II which causes the change of the defect concentration is immobile, thus the step-like defect concentration profile is not subject to any change with time.

The length of both crystals along the z-axis is denoted as Δz^{I} and Δz^{II}, and the ratio $a_z \equiv \Delta z^{\mathrm{II}}/(\Delta z^{\mathrm{I}} + \Delta z^{\mathrm{II}})$ indicates the volume fraction of region II of the bicrystal. If we assume that the heat conductivities of phases I and II are equal, the total temperature difference ΔT is split of between I and II according to the geometric fraction a_z, i.e. $\Delta T^{\mathrm{I}} = (1-a_z)\Delta T$ and $\Delta T^{\mathrm{II}} = a_z \Delta T$.

Modifying Eq. (4), we thus have

$$\mathrm{d}\varphi = \frac{1}{F} \cdot [\mathrm{d}\tilde{\mu}^{\mathrm{I}}_{\mathrm{A}} + \mathrm{d}\tilde{\mu}^{\mathrm{II}}_{\mathrm{A}^+} - \mathrm{d}\mu_{\mathrm{A}}(\mathrm{A}) + \mathrm{d}\tilde{\mu}_{e'}(\mathrm{Pt})]. \tag{26}$$

With Eq. (9) this leads to

$$\mathrm{d}\varphi = \frac{1}{F} \cdot [-S^{*,\mathrm{I}}_{\mathrm{A}^+}\mathrm{d}T^{\mathrm{I}} - S^{*,\mathrm{II}}_{\mathrm{A}^+}\mathrm{d}T^{\mathrm{II}} + S^{\circ}_{\mathrm{A}}\mathrm{d}T + \mathrm{d}\tilde{\mu}_{e'}(\mathrm{Pt})] \tag{27}$$

and by taking our assumption on ∇T into account results in

$$\mathrm{d}\varphi = \frac{1}{F} \cdot [-(1-a_z)S^{*,\mathrm{I}}_{\mathrm{A}^+}\mathrm{d}T - a_z S^{*,\mathrm{II}}_{\mathrm{A}^+}\mathrm{d}T + S^{\circ}_{\mathrm{A}}\mathrm{d}T + \mathrm{d}\tilde{\mu}_{e'}(\mathrm{Pt})]. \tag{28}$$

Using the definition of the ionic thermopower in Eq. (10), we finally obtain

$$\epsilon^{\mathrm{I,II}}_{\perp} = \frac{\mathrm{d}\varphi}{\mathrm{d}T} = (1-a_z)\epsilon^{\mathrm{I}}_{\mathrm{A}^+} + a_z\epsilon^{\mathrm{II}}_{\mathrm{A}^+} - \epsilon_{e'}(\mathrm{Pt}) \tag{29}$$

which describes the operationally defined thermopower of the thermogalvanic cell in Fig. 5. By subtracting $\epsilon^{\#}$, i.e. the thermopower of a thermocell consisting of pure AX ($a_z = 0$), the volume fraction weighted difference between the absolute thermopower of doped and pure AX,

$$\Delta\epsilon^{\mathrm{I,II}}_{\mathrm{A}^+,\perp} = a_z(\epsilon^{\mathrm{II}}_{\mathrm{A}^+} - \epsilon^{\#}_{\mathrm{A}^+}) \tag{30}$$

results. Obviously the thermopower of the bicrystal is dominated by the more extended phase. Inserting Eq. (17) into Eq. (30) and assuming that the values for A, B, C and ψ_{i} are independent of α_{i}, we obtain

$$\Delta\epsilon^{\mathrm{I,II}}_{\mathrm{A}^+,\perp} = -\frac{a_z}{F} \cdot \left[\frac{A}{T}(\tanh\ln\psi_{\mathrm{i}}^{1/2}\alpha_{\mathrm{i}}^{\mathrm{II}} - \tanh\ln\psi_{\mathrm{i}}^{1/2}) - R\ln\alpha_{\mathrm{i}}^{\mathrm{II}}\right] \tag{31}$$

By the subtraction of the thermopower of the pure AX crystal, the constant but unknown terms B and C, the entropy of the electrode metal and the thermopower of the platinum leads cancel. Regarding the doped phase II as a disturbance of an otherwise pure crystal AX, the difference $\Delta\epsilon^{\mathrm{I,II}}_{\mathrm{A}^+,\perp}$ depends on two factors: It depends linearly on the extension of region II, which is known. And once the terms $A = (Q^*_{\mathrm{i}} + Q^*_{\mathrm{v}} + \Delta H^{\circ}_{\mathrm{F}})/2$ and ψ_{i} are known, the concentration $\alpha^{\mathrm{II}}_{\mathrm{i}}$ can be extracted from the experimental determination of $\Delta\epsilon^{\mathrm{I,II}}_{\mathrm{A}^+,\perp}$.

In Fig. 6, the thermopower difference is calculated for various simple cases. Necessarily the difference vanishes for $\alpha^{\mathrm{II}}_{\mathrm{i}} = 1$, i.e. for a bicrystal consisting of two identical pure crystallites. If region II is doped such that the concentration of vacancies is increased ($\alpha^{\mathrm{II}}_{\mathrm{i}} < 1$), the difference becomes positive. If region II has interstitial concentration ($\alpha^{\mathrm{II}}_{\mathrm{i}} > 1$) the difference becomes negative. Obviously this simple behavior is only observed for values of ψ_{i}, close to 1.

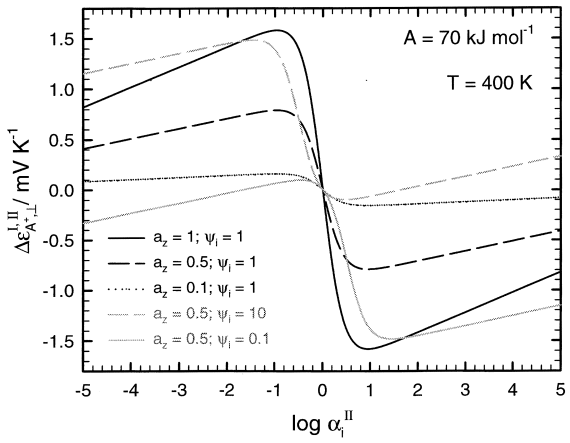

Fig. 6. Difference between the thermopower of the bicrystal (interface perpendicular to the temperature gradient) in Fig. 5 and a pure crystal of the same size as a function of the degree of doping in region II of the bicrystal, calculated with Eq. (31).

Low (high) values of ψ_i lead to a shift of $\Delta\epsilon^{I,II}_{A^+,\perp}$ to more negative (positive) values. Quite simply, the curve in Fig. 6 reflects the concentration dependence of the ionic thermopower which is shown in Fig. 2.

Summarizing, the bicrystal can be regarded as two thermobatteries being connected in series, with the total thermopower as the volume weighted sum of the thermopowers of each region of the bicrystal [27] ($V = \Delta x \cdot \Delta y \cdot \Delta z$),

$$\epsilon_{A^+,\perp} = \frac{V^I}{V^I + V^{II}} \cdot \epsilon^I + \frac{V^{II}}{V^I + V^{II}} \cdot \epsilon^{II} = (1 - a_z)\epsilon^I_{A^+} - a_z \epsilon^{II}_{A^+}. \quad (32)$$

2.5. Thermopower of a bicrystal with its interface parallel to the temperature gradient

In Fig. 7, the experimental arrangement of a bicrystal $AX(\alpha^I_i = 1)|AX(\alpha^{II}_i \neq 1)$ with its interface parallel to the temperature gradient ∇T is depicted, together with its representation in terms of a simple electric circuit.

From the condition of zero total electric current across the total area $\Sigma_i A^i_{cr}$ of the bicrystal under open circuit condition

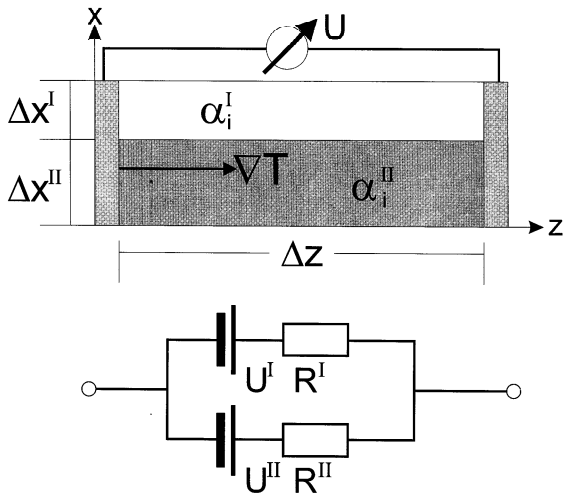

Fig. 7. A bicrystal (interface parallel to the temperature gradient) composed of two ionic crystals AX with different defect concentrations. Region I contains no impurities (intrinsic disorder, $\alpha^I_i = 1$). Region II is homogeneously doped ($\alpha^{II}_i \neq 1$).

$$I = \sum_i I^i = 0 \quad (33)$$

it follows for the current densities j_i in both half crystals

$$\sum_i I^i = F \cdot \sum_i j^i A^i_{cr} = 0. \quad (34)$$

The sectional cross areas A^I_{cr} and A^{II}_{cr} of the two regions are given as

$$A^I_{cr} = \Delta y \cdot \Delta x^I \quad \text{and} \quad A^{II}_{cr} = \Delta y \cdot \Delta x^{II} \quad (35)$$

and Eq. (33) leads with the definition of the volume fraction $\alpha_x = \Delta x^{II}/(\Delta x^I + \Delta x^{II})$ to

$$0 = (1 - a_x) \cdot j^I_{A^+} + a_x \cdot j^{II}_{A^+} \quad (36)$$

Inserting the flux Eq. (8) into Eq. (36) one obtains

$$0 = (1 - a_x) \cdot L^I_{A^+}[\nabla\tilde{\mu}^I_{A^+} + S^{*,I}_{A^+} \cdot \nabla T^I] + a_x \cdot L^{II}_{A^+}[\nabla\tilde{\mu}^{II}_{A^+} + S^{*,II}_{A^+} \cdot \nabla T^{II}] \quad (37)$$

Assuming again that $\nabla T^I = \nabla T^{II} = \nabla T$, i.e. that both phases have identical heat conductivities, and that local equilibrium prevails at the boundary between the two crystals, i.e. $\nabla\tilde{\mu}^I_{A^+} = \nabla\tilde{\mu}^{II}_{A^+} = \nabla\tilde{\mu}_{A^+}$, it follows for $\nabla\tilde{\mu}_{A^+}$

$$\nabla\tilde{\mu}_{A^+} = -\left[\frac{(1 - a_x) \cdot L^I_{A^+}}{(1 - a_x) \cdot L^I_{A^+} + a_x \cdot L^{II}_{A^+}} \cdot S^{*,I}_{A^+} + \frac{a_x \cdot L^{II}_{A^+}}{(1 - a_x) \cdot L^I_{A^+} + a_x \cdot L^{II}_{A^+}} \cdot S^{*,II}_{A^+}\right] \nabla T \quad (38)$$

Introducing the thermopower (Eqs. (7) and (10)) and subtracting the thermopower of a thermogalvanic cell composed of a pure crystal of the same size we obtain:

$$\Delta\epsilon^{I,II}_{A^+,||} = \frac{a_x \cdot L^{II}_{A^+}}{(1 - a_x) \cdot L^I_{A^+} + a_x \cdot L^{II}_{A^+}} \cdot (\epsilon^{II}_{A^+} - \epsilon^{\neq}_{A^+}) \quad (39)$$

Inserting Eq. (15) for the transport coefficient L_{A^+} of the ions and Eq. (17) for the ionic thermopower one ends with

$$\Delta\epsilon^{\mathrm{I,II}}_{\mathrm{A}^+,||} = -\frac{1}{F}\cdot\frac{a_x\cdot[\psi_\mathrm{i}\alpha_\mathrm{i}^{\mathrm{II}}+(\alpha_\mathrm{i}^{\mathrm{II}})^{-1}]}{(1-a_x)\cdot(\psi_\mathrm{i}+1)+a_x\cdot[\psi_\mathrm{i}\alpha_\mathrm{i}^{\mathrm{II}}+(\alpha_\mathrm{i}^{\mathrm{II}})^{-1}]} \cdot\left[\frac{A}{T}\cdot(\tanh\ln\psi^{1/2}\alpha_\mathrm{i}^{\mathrm{II}}-\tanh\ln\psi^{1/2})-R\ln\alpha_\mathrm{i}^{\mathrm{II}}\right] \quad (40)$$

In Fig. 8 numerical results from Eq. (40) are depicted. As in the case of the perpendicular bicrystal arrangement, vacancy doping in region II leads to positive differences $\Delta\epsilon^{\mathrm{I,II}}_{\mathrm{A}^+,||}$. Values of $\psi_\mathrm{i}>1$ ($\psi_\mathrm{i}<1$) lead to a shift of $\Delta\epsilon^{\mathrm{I,II}}_{\mathrm{A}^+,||}$ to more positive (negative) values. The general appearance of the curves is similar to those in Fig. 6. However, comparing identical bicrystals we find that the thermopower difference is more pronounced in the parallel arrangement. Furthermore, whereas the curves in Fig. 6 simply reflect the $\tanh\ln\alpha_\mathrm{i}$-dependence of Eq. (31), the curves in Fig. 8 show a more complicate shape.

The two crystals can be regarded as two thermobatteries being connected in parallel, with the total thermopower as a conductivity (σ) and volume (V) weighted mean value of the thermopower of each region of the bicrystal [27]

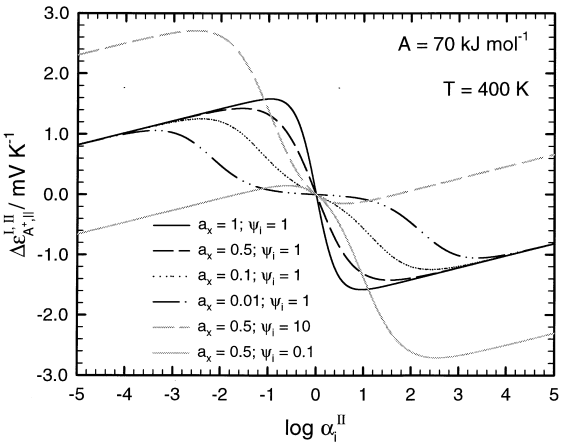

Fig. 8. Calculated differences between the thermopower of the bicrystal (interface parallel to the temperature gradient) in Fig. 7 and a pure crystal AX of the same size as a function of doping in region II of the bicrystal, according to Eq. (40).

$$\epsilon_{||} = \frac{\sigma^{\mathrm{I}}V^{\mathrm{I}}}{\sigma^{\mathrm{I}}V^{\mathrm{I}}+\sigma^{\mathrm{II}}V^{\mathrm{II}}}\cdot\epsilon^{\mathrm{I}}+\frac{\sigma^{\mathrm{II}}V^{\mathrm{II}}}{\sigma^{\mathrm{I}}V^{\mathrm{I}}+\sigma^{\mathrm{II}}V^{\mathrm{II}}}\cdot\epsilon^{\mathrm{II}}. \quad (41)$$

Thus, in a temperature gradient an electric ring current is induced whenever two phases with different thermopowers are exposed to a temperature gradient in parallel.

2.6. Thermopower of a single space charge layer perpendicular to ∇T

In the following, we calculate the thermopower of an inhomogeneously doped AX crystal. The dopant concentration profile is given by Eq. (22), i.e. it corresponds directly to the defect concentration profile within a space charge layer. Again we assume that this profile is not subject to a change with time. Since Eq. (17) is valid as long as the Frenkel equilibrium is obeyed, the origin of the deviation of the defect concentrations from their intrinsic values is irrelevant. Thus, the combination of Eq. (17) with the concentration function in Eq. (22) allows the evaluation of the thermopower of space charge regions.

To calculate the thermopower of an inhomogeneous crystal we have to change from a summation over the two parts of a bicrystal to an integration over the corresponding space coordinate. Starting with Eq. (9) in terms of the gradients of the electrochemical potential of the ions and the temperature gradient, we integrate over the normalized space coordinate $\zeta\equiv z/\lambda_\mathrm{D}$ which represents the z-coordinate divided by the Debye length λ_D:

$$\int_0^{\Delta\zeta}\nabla\tilde{\mu}_{\mathrm{A}^+}\mathrm{d}\zeta = -\int_0^{\Delta\zeta}(S^*_{\mathrm{A}^+}\cdot\nabla T)\mathrm{d}\zeta \quad (42)$$

Assuming a spatially homogeneous temperature gradient given by $\nabla T=\Delta T/\Delta\zeta$ we obtain

$$\Delta\tilde{\mu}_{\mathrm{A}^+} = -\frac{\Delta T}{\Delta\zeta}\int_0^{\Delta\zeta}S^*_{\mathrm{A}^+}\mathrm{d}\zeta \quad (43)$$

The combination of Eq. (43) with Eqs. (5), (7), (10) results in the thermopower of the cell arrangement in Fig. 9:

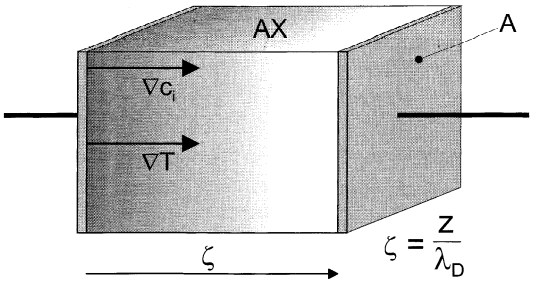

Fig. 9. A crystal AX with an inhomogeneous dopant concentration profile. The temperature gradient runs perpendicular to the iso-concentration planes.

$$\epsilon_{\perp} = \frac{1}{\Delta\zeta}\int_0^{\Delta\zeta} \epsilon_{A^+}(\zeta)\mathrm{d}\zeta - \epsilon_{e'}(\mathrm{Pt}) \tag{44}$$

Subtracting the thermopower $\epsilon^{\#}$ of a pure crystal we obtain

$$\begin{aligned}\Delta\epsilon_{A^+,\perp} &= \int_0^{\Delta\zeta} \epsilon_{A^+}(\zeta)\frac{\mathrm{d}\zeta}{\Delta\zeta} - \epsilon^{\#}_{A^+}\frac{\Delta\zeta}{\Delta\zeta} \\ &= \frac{1}{\Delta\zeta}\int_0^{\Delta\zeta} [\epsilon_{A^+}(\zeta) - \epsilon^{\#}_{A^+}]\,\mathrm{d}\zeta \end{aligned} \tag{45}$$

Inserting Eq. (17) one obtains

$$\begin{aligned}\Delta\epsilon_{A^+,\perp} = -\frac{1}{F\Delta\zeta} \cdot \Bigg[\frac{A}{T}\cdot\Bigg(\int_0^{\Delta\zeta} \tanh\ln\psi_i^{1/2}\alpha_i(\zeta)\mathrm{d}\zeta \\ - \int_0^{\Delta\zeta} \tanh\ln\psi_i^{1/2}\mathrm{d}\zeta\Bigg) - R\int_0^{\Delta\zeta}\ln\alpha_i(\zeta)\mathrm{d}\zeta\Bigg]\end{aligned} \tag{46}$$

With $\alpha_i(\zeta)$ as given by Eq. (22) for the defect concentration profile in a space charge layer, all integrals in Eq. (46) are solved analytically (see Appendix (A.3)). Numerical integration has been performed to check the solutions for correctness. In Fig. 10, numerical results calculated from Eq. (46) are depicted.

Firstly the thermopower difference is not a linear

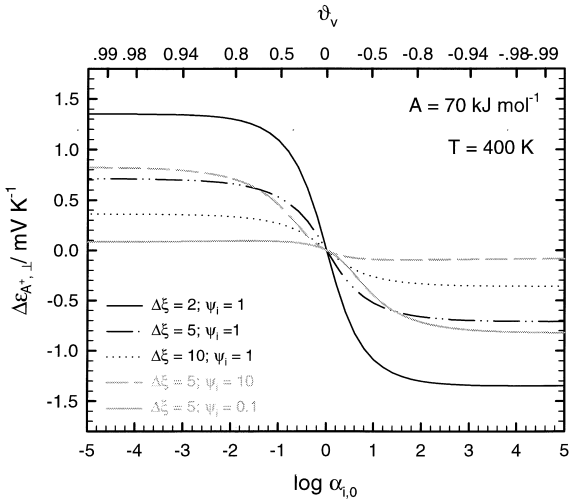

Fig. 10. Calculated differences between the thermopower of an inhomogeneous crystal (perpendicular case) in Fig. 9 and a pure crystal as a function of the normalized interstitial concentration $\alpha_{i,0}$ in the crystal layer next to the interface. The calculation is based on Eq. (46) and its solution in Appendix (A.3).

function of the length of the crystal. Only for mobility ratios close to $\psi_i = 1$ does the thermopower difference show a symmetric behavior around $\alpha_{i,0} = 1$. For $\alpha_{i,0} < 0.01$ or $\alpha_{i,0} > 100$ the thermopower difference tends to asymptotic values. This can be explained by a saturation effect in the space charge region, expressed by an almost constant ϑ_v value, together with the extrema in the concentration dependence of the thermopower (see Fig. 2). For a comparison of the inhomogeneous system with a bicrystal a mean defect concentration and a typical thickness of the space charge layer can be introduced. According to Maier an effective thickness of the space charge layer is given by 2 λ_D. In the case of isothermal systems, the mean concentration is well represented by the geometric mean of the concentration in the bulk and directly at the interface of the dopant grain [28]:

$$a_z = 2/\Delta\zeta \quad \alpha_i^{II} = \sqrt{\alpha_{i,0}\cdot\alpha_i^{\#}} \tag{47}$$

In Fig. 11 we compare the results from the exact solution with results from the approximate (isothermal) bicrystalline solution (Eq. (47)). The approximation works well for mobility ratios close to 1 and not too large or small values of $\alpha_{i,0}$. For $\psi_i > 1$

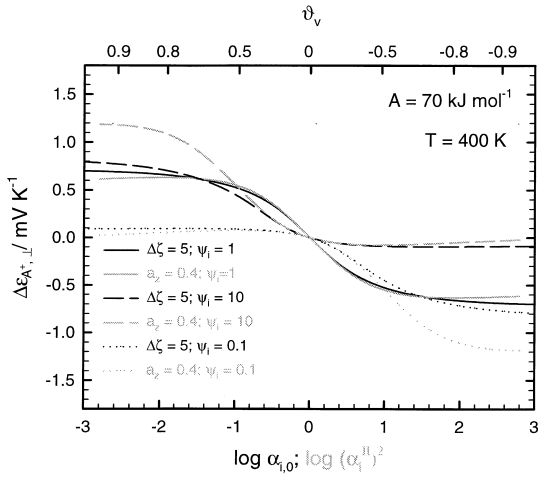

Fig. 11. Comparison of numerical results for the thermopower difference of an inhomogeneous crystal (perpendicular case) and a bicrystal, being composed of pure AX and homogeneously doped AX($\alpha_i^{II}=\sqrt{\alpha_{i,0}\alpha_i^{\#}}$) (with $\alpha_i^{\#}=1$; bicrystal = grey lines, inhomogeneous crystal = black lines).

the thermopower difference is shifted to more positive values, whereas the thermopower difference is shifted to more negative values for $\psi_i<1$. In essence the simple geometric mean value of α_i is not suitable for the bicrystalline approximation if ψ_i differs significantly from 1. The failure of the geometric mean for the description of an non-isothermal space charge layer is due to the more complicated integrals of the defect concentrations in Eq. (46).

2.7. Thermopower of a single space charge layer parallel to ∇T

In Fig. 12, the arrangement of a crystal with an inhomogeneous dopant profile with its isoconcentration planes parallel to ∇T is shown schematically. The crystal direction parallel to the direction of the concentration gradient is denoted as $\xi=x/\lambda_D$. As in the case of a bicrystal, a temperature gradient parallel to the isoconcentration planes induces ring currents in the specimen. The inhomogeneous crystal can be described as an infinite number of small thermobatteries with different thermopowers and internal resistance, being connected in parallel.

To evaluate $\Delta\epsilon_{A^+,||}$ we start with the condition of a zero total current through the cross section of the inhomogeneous crystal as in Eqs. (33) and (34). The

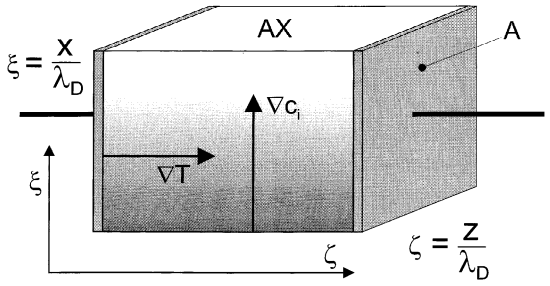

Fig. 12. A crystal AX with an inhomogeneous dopant concentration profile. The temperature gradient runs parallel to the isoconcentration planes.

integration over the normalized space variable $\xi=x/\lambda_D$ and subtraction of the thermopower of a pure crystal leads to an integral form of Eq. (39):

$$\Delta\epsilon_{A^+,||} - \frac{\int_0^{\Delta\xi} L_{A^+}(\xi)\cdot[\epsilon_{A^+}(\xi)-\epsilon_{A^+}^{\#}]d\xi}{\int_0^{\Delta\xi} L_{A^+}(\xi)d\xi} \tag{48}$$

Inserting Eq. (15) for the transport coefficient L_{A^+} of the ions and Eq. (17) for the ionic thermopower one ends with

$$\begin{aligned}\Delta\epsilon_{A^+,||} = & -\frac{1}{F} \\ & \cdot\left\{\int_0^{\Delta\xi}[\psi_i\alpha_i(\xi)+(\alpha_i(\xi))^{-1}]\cdot\left[\frac{A}{T}\right.\right. \\ & \cdot(\tanh\ln\psi^{1/2}\alpha_i(\xi)-\tanh\ln\psi^{1/2}) \\ & \left.\left.-R\ln\alpha_i(\xi)\right]d\xi\right\}/\left\{\int_0^{\Delta\xi}[\psi_i\alpha_i(\xi)\right. \\ & \left.+(\alpha_i(\xi))^{-1}]d\xi\right\}\end{aligned} \tag{49}$$

Using Eq. (22) for the concentration profile $\alpha_i(\xi)$ all integrals are solved analytically and numerically (see Appendix (A.4)).

The calculated thermopower difference in Fig. 13 shows the same shape as in the case of a bicrystal (see Fig. 8). If the defect adsorption at the interface

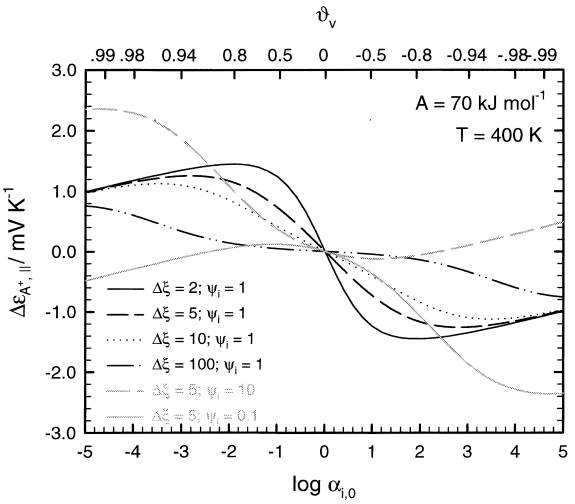

Fig. 13. Calculated differences between the thermopower of the inhomogeneous crystal (parallel case) in Fig. 12 and a pure crystal as a function of the normalized interstitial concentration $\alpha_{i,0}$ in the crystal layer next to the interface. The calculation is based on Eq. (49) and its solution in Appendix (A.4).

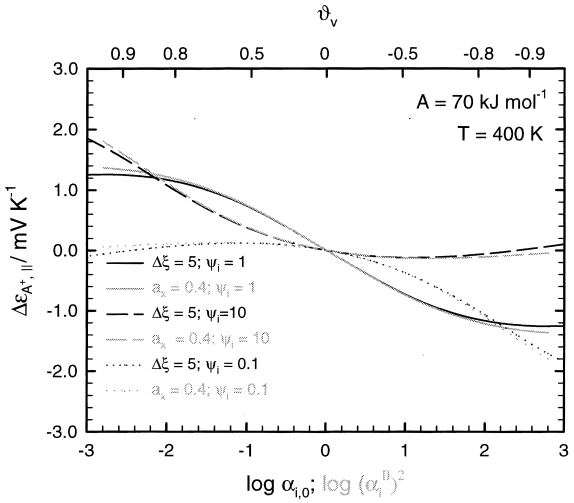

Fig. 14. Comparison of numerical results for the thermopower difference of an inhomogeneous crystal (parallel case) and a bicrystal, being composed of pure AX and AX($\alpha_i^{II}=\sqrt{\alpha_{i,0}\alpha_i^{\#}}$) (with $\alpha_i^{\#}=1$; bicrystal = grey lines, inhomogeneous crystal = black lines).

is not too strong, the thermopower of the inhomogeneous crystal can be approximated by the thermopower of a bicrystal, using a mean defect concentration and thickness (Eq. (47)). A comparison of the results from Eq. (47) and the bicrystalline approximation is depicted in Fig. 14. As expected, the thermopower difference increases strongly with decreasing $\Delta\xi$, i.e. with an increasing Debye length. The thermopower difference is shifted to more positive values for mobility ratios $\psi_i > 1$. As indicated in Fig. 13 a mobility ratio $\psi_i = 10$ shifts the thermopower difference almost completely to positive values. Correspondingly, mobility ratios $\psi_i < 1$ lead to a shift of $\Delta\epsilon_{A^+,||}$ to negative values. For real systems the mobility ratio will always be different from unity and thus, $\Delta\epsilon_{A^+,||}$ will always be shifted either to positive or negative values.

2.8. Thermopower of composites

It is virtually impossible to describe the real morphology of a dispersed solid electrolyte in analytical terms. Thus, one has to approximate the distribution of the space charge layers by geometric models that can be calculated analytically. The ‘‘brick layer’’ model is based on a regular distribution of insulator cubes and is thus represented by a three-dimensional network of interfaces parallel and perpendicular to the temperature gradient. It has been successfully applied to the calculation of the conductivity of heterogeneous solid electrolytes by Maier [29]. Yoo et al. applied a brick layer model to the calculation of the electric thermopower of homogeneous composites of n- and p-type semiconductors [27], without the consideration of inhomogeneous regions.

The brick layer model represents a serial and parallel network of equivalent dopant particles. In a temperature gradient each insulator grain and the surrounding space charge layers can be regarded as a local thermobattery. The parallel connection of such batteries, having the same thermovoltage, does not change the measurable total voltage. The serial connection of thermobatteries results in a voltage of $U = N \cdot U^{\text{grain}} = N \cdot \epsilon^{\text{grain}} \Delta T^{\text{grain}} = \epsilon \cdot \Delta T$. Thus the thermopower of one grain and its surrounding electrolyte phase equals the total thermopower of the system, if the temperature gradient ∇T is assumed to be locally homogeneous.

Assuming a cubic geometry for the insulator particles (Fig. 15), a most simple model composite can be represented by an electric circuit consisting of

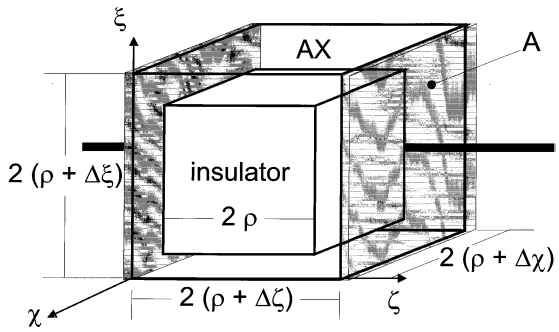

Fig. 15. The composite material is regarded as being composed of equally sized insulator particles embedded in the solid electrolyte. The cubic insulator particle is surrounded by space charge layers at all its surfaces.

parallel and serial connections as depicted in Fig. 16. The normalized length of the dopant grain is 2ρ, the extension of the grain together with its space charge layers is defined as $2(\Delta\xi+\rho)=2(\Delta\zeta+\rho)=2(\Delta\chi+\rho)$.

All space charge layers have the same composition and the same size. Furthermore interactions between the different parts of the space charge layer around a grain are neglected, i.e. the space over the vertices gives no contribution to the thermopower. Definitely, this is a rough approximation but will not lead to qualitative errors. The parallel connection of the (parallel) space charge layers can be reduced to a single parallel space charge layer ($U_{||}=\epsilon_{A^+,||}\cdot\Delta T$).

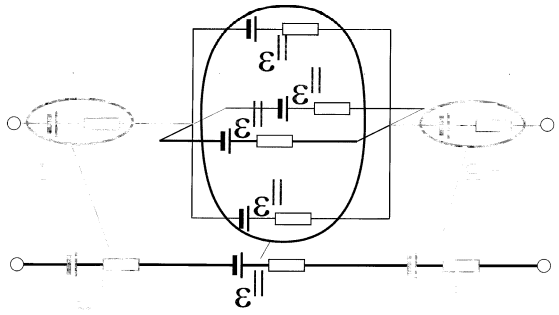

Fig. 16. An equivalent electric network describing the electric behavior of the unit thermogalvanic cell in Fig. 15. The network can be reduced to a serial connection of two different thermocells (parallel and perpendicular space charge layers).

The two interfaces perpendicular to the temperature gradient contribute equally to the total thermopower. Thus the total thermopower is calculated as the sum of the contributions of two surfaces perpendicular and a surface parallel to the temperature gradient. The situation is simplified by the fact that the temperature difference along the cell is small, and thus, the temperature dependence of the thermopower can be neglected. Assuming a constant temperature gradient, the total temperature difference can be split up according to the geometric fraction of the different crystal regions and we obtain:

$$\epsilon_{A^+} = \epsilon_{A^+,\perp}(\Delta\zeta)\cdot\frac{\Delta\xi}{\Delta\xi+\rho} + \epsilon_{A^+,||}(\Delta\xi)\cdot\frac{\rho}{\Delta\xi+\rho} \tag{50}$$

In order to express Eq. (50) in terms of the volume fraction ϕ of the dopant, $2\,\Delta\xi$ is identified as the distance between two dopant grains. Assuming cubic dopant grains the volume fraction of dopant results as

$$\phi = \frac{V_{dop}}{V_{tot}} = \frac{r_A^3}{a_{tot}^3} = \frac{\rho^3}{(\rho+\Delta\xi)^3}. \tag{51}$$

Vice versa $\Delta\xi$ can be expressed as

$$\Delta\xi = \Delta\zeta = \Delta\chi = \rho\cdot(\phi^{-1/3}-1). \tag{52}$$

With Eq. (52) the Eq. (50) can be transformed to

$$\epsilon_{A^+} = \epsilon_{A^+,\perp}(\Delta\zeta)\cdot(1-\phi^{1/3}) + \epsilon_{A^+,||}(\Delta\xi)\cdot\phi^{1/3} \tag{53}$$

Since $\epsilon_{A^+,\perp}$ and $\epsilon_{A^+,||}$ are themselves functions of $\Delta\zeta$ and $\Delta\xi$, no simple relation for the volume dependence can be derived.

Numerical results for the thermopower of $AgCl:Al_2O_3$ as a model system are depicted in Fig. 17 as a function of temperature for four different volume fractions ϕ, applying Eqs. (46), (49), (53).

The necessary parameters A, B, C and ψ_i are taken from Christy [11] and Teltow [18], thus are the same as those used for the calculation of the curves in Fig. 3. We thereby assume that ΔH_F°, S_i°, S_v°, Q_i^*, Q_v^*, ψ_i, and their temperature dependence, as determined for

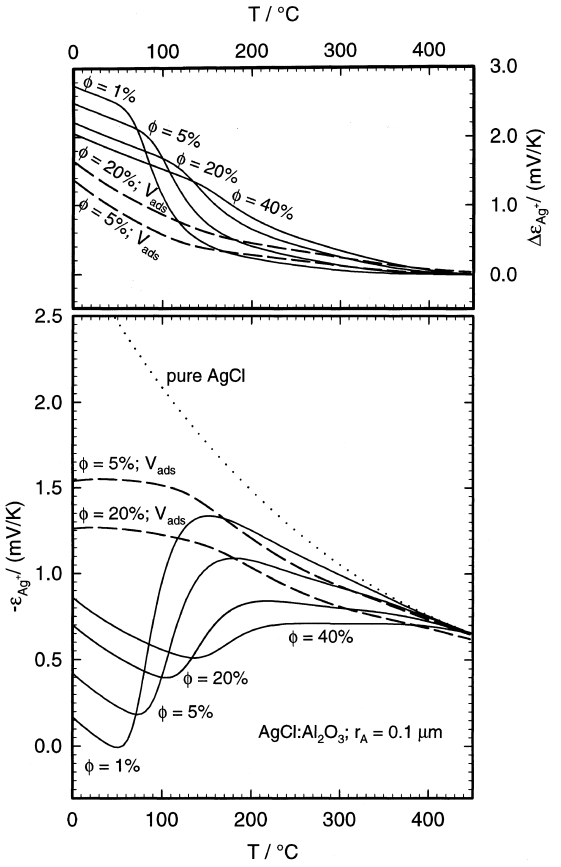

Fig. 17. Calculated temperature dependence of the thermopower ϵ_{Ag^+} and the thermopower difference of $\Delta\epsilon_{Ag^+}$ of AgCl:Al_2O_3-composites. The different parameters in Eq. (17) are taken from Christy [11], the temperature dependence of $\alpha_{i,0}$ is taken from Maier [2]. Data for the hypothetical adsorption of vacancies (V_{Ads}) are represented by dashed lines.

homogeneous (Ag,Cd)Cl, are also valid for the composite material (see discussion of this assumption in Section 4). The adsorption equilibrium is incorporated via the temperature dependent parameter $\alpha_{v,0}$ as given by Eq. (25) [2].

The results for the temperature dependence of ϵ_{Ag^+} are comparable to those for homogeneously doped material in Fig. 3. A broad maximum which depends in position and height on the degree of doping is obtained. It indicates the onset of the extrinsic regime with decreasing temperature and can be taken as a measure of the dopant concentration (volume fraction). At even lower temperatures the thermopower increases again, leading to a pronounced minimum.

Comparing Figs. 3 and 17 more closely one has to conclude that a thermopower study will probably not allow a decision on whether the material is doped homogeneously or heterogeneously. Rather, the temperature dependence is virtually identical in shape for both cases. Nevertheless, the calculated data suggest that the thermopower extrema of composites occur typically at lower temperatures than those of homogeneously doped materials. Thus, whereas the thermopower of $CdCl_2$-doped AgCl shows a considerable concentration dependence at 300°C, the dispersion of Al_2O_3 has less effect at the same temperature. This coincides with the results from conductivity measurements on homogeneously and heterogeneously doped materials.

Additional data are depicted in Fig. 17 for the hypothetical case of vacancy depletion in the space charge layers. We arbitrarily chose a free enthalpy for the adsorption of vacancies, being identical to that for the adsorption of ions (see Eq. (25)). The smaller one chooses this adsorption enthalpy, the closer come the thermopower data to the data for pure material. At higher temperatures the calculated data are virtually identical to the case of interstitial depletion which would prevent a distinction of both cases by a thermopower measurement. The reason for this behavior is the magnitude of $\vartheta\psi_i$. It is considerably larger than 1, and thus, as can be seen in Figs. 6, 8, 10 and 13, both the introduction of additional interstitials or vacancies (with different concentrations) may lead to comparable (equally signed) thermopower changes.

In Fig. 18, the calculated dependence of ϵ_{Ag^+} on the volume fraction ϕ of Al_2O_3 is depicted. A maximum results at a volume fraction that depends strongly on temperature. With increasing temperature the maximum thermopower occurs at higher volume fraction, which is necessary to compensate the higher intrinsic defect concentration (smaller λ_D) by a larger geometric contribution of space charge regions.

At a given volume fraction and temperature, the thermopower depends also strongly on the average grain diameter $2\cdot r_A$ of Al_2O_3. In general, the thermopower difference $\Delta\epsilon_{Ag^+}$ decreases with increasing grain size. At low temperature, a maximum

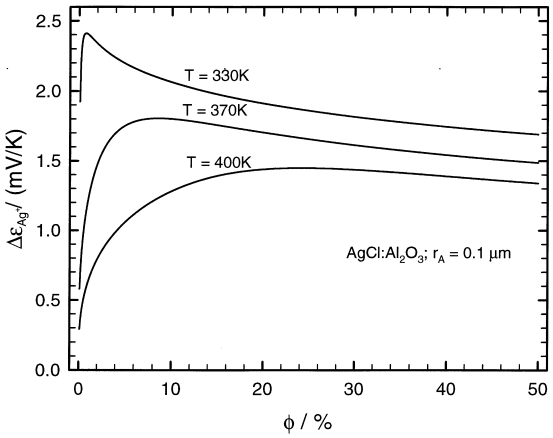

Fig. 18. Calculated dependence of $\Delta\epsilon_{Ag^+}$ of AgCl:Al_2O_3-composites on the volume fraction ϕ of Al_2O_3.

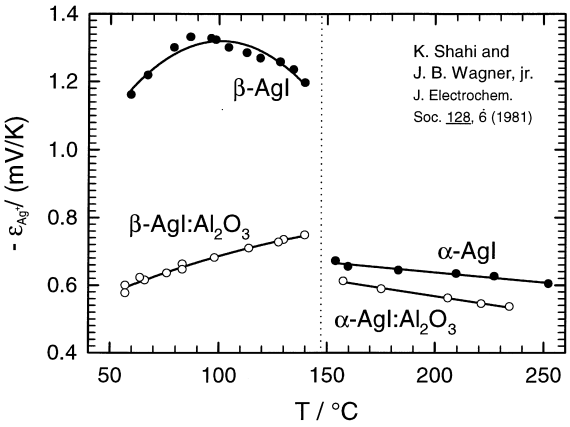

Fig. 20. Thermopower of α-AgI:Al_2O_3 and β-AgI:Al_2O_3 dispersions and of pure AgI as a function of temperature; data taken from [14].

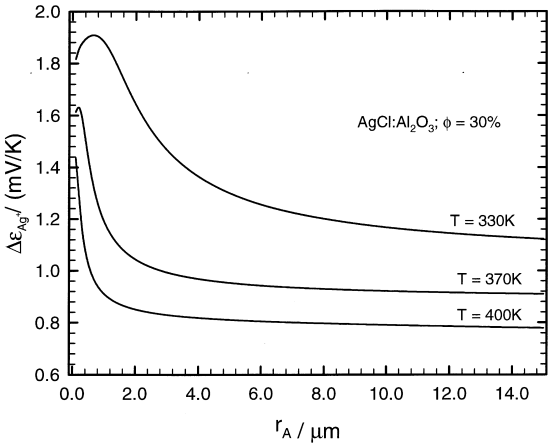

Fig. 19. Calculated dependence of $\Delta\epsilon_{Ag^+}$ of AgCl:Al_2O_3-composites on the grain radius of Al_2O_3.

effect exists at a grain diameter in the order of 1 μm, see Fig. 19.

3. Experiments

As indicated only a minor number of experimental data exist so far for the thermopower of solid electrolyte composites. In Fig. 20, the experimental results of Shahi and Wagner for the thermopower of pure AgI and AgI:Al_2O_3 composites are depicted for comparison with our formal results in Fig. 17. To our knowledge, no other data for the thermopower of electrolyte composites have been reported to date.

The measurements extend over a relatively wide temperature range from $T = 55$°C to $T = 255$°C and include both the α- and the β-phase of AgI. As one might expect from the high degree of intrinsic disorder, the (negative) thermopower of the (high-T) α-phase is not seriously affected by the dispersion of alumina particles. In contrast to this, the (negative) thermopower of the (low-T) β-phase with cation Frenkel disorder is reduced considerably.

In the light of the previous formal considerations and numerical calculations, the measured change of the thermopower of β-AgI upon dispersing Al_2O_3 can be interpreted as the effect of space charge regions with an increased concentration of cation vacancies. Since we have no information on the interfacial chemistry of the β-AgI:Al_2O_3 system, it is difficult to draw further quantitative conclusions. However, comparing the results for β-AgI in Fig. 20 with the calculations for AgCl in Fig. 17, our calculations are at least in qualitative agreement with the experimental findings: Firstly the thermopower of pure β-AgI exhibits a maximum around $T = 100$°C

which has to be explained by homogeneously distributed impurities, i.e. the extrinsic defect region is approached with decreasing temperature (cf. Fig. 3). On dispersing Al_2O_3, the thermopower ϵ_{Ag^+} decreases strongly. Furthermore, Shahi and Wagner find an increase of $-\epsilon_{A^+}$ with increasing temperature which is a clear indication of a dopant effect, since the thermopower $-\epsilon_{A^+}$ of pure material is always decreasing hyperbolically with increasing temperature. Regarding Fig. 17, this increase of ϵ_{Ag^+} might be explained by a virtual maximum at a higher temperature outside the phase field of β-AgI, caused by serious heterogeneous doping and the presence of space charge regions.

In a recent experimental study Lee and Maier [30] question the ideal space charge model for AgI:Al_2O_3 composites and suggest that the conductivity enhancement in β-AgI:Al_2O_3 dispersions is due to the presence of a second electrolyte phase with different crystallographic properties around the alumina grains. New experiments show that a 7H-phase with stacking fault arrangement is formed which can be conceived as a nano-sized multilayer (γ-β-γ-...) of two different AgI phases [31]. This phase will most probably exhibit a different defect structure than pure β-AgI and could thus also explain a change in the ionic thermopower of the composite. As is shown by our comparison of inhomogeneous and bicrystalline specimens, thermopower measurements will not allow us to decide between the space charge model and the occurrence of a second phase as possible explanations of an excess conductivity.

Our own thermopower measurements on the composite α-$Ag_{2+\delta}S$:Al_2O_3 (5 vol%) [32] and pure α-$Ag_{2+\delta}S$ [25,33] at $T = 169$°C show no difference within the experimental error. This is probably due to the high intrinsic defect concentrations, leading to a Debye length of $\lambda_D \simeq 4$Å. At lower temperatures, which were required in order to reduce the intrinsic defect concentrations, it was difficult to equilibrate the nonstoichiometric α-$Ag_{2+\delta}S$:Al_2O_3 specimens, and thus, we failed to measure the thermopower at lower temperatures.

Our own preliminary measurements on AgCl show considerable changes of the ionic thermopower on incorporating Al_2O_3. However, different Al_2O_3 material supplied by different companies gives different results and so far no systematic conclusion can be drawn. A more comprehensive experimental study of the ionic thermopower of AgCl:Al_2O_3 and other composite electrolytes is in progress.

4. Discussion

In the previous sections we analyzed the ionic thermopower of inhomogeneous electrolyte regions and of electrolyte composites on the basis of a simple lattice point defect model and the available solution of the Poisson-Boltzmann equation [5–8]. We showed that the isothermal solution is valid also for the non-isothermal case, if the degree of adsorption is not too small. As in the interpretation of ionic conductivity measurements, only a few defect parameters are necessary for a semi-quantitive understanding. Assuming the validity of the space charge model, thermopower measurements provide in general a means to decide whether the dispersion of an inert phase leads to the creation of either additional interstitial or vacancy defects. However one has to be very careful in applying too simple rules for this decision. Depending on the degree of impurity content and temperature, the thermopower of nearly intrinsic material can take both positive or negative values, depending crucially on the mobility ratio. Only for mobility ratios close to 1 is the thermopower positive (negative) if vacancies (interstitials) are added to the crystal. Thus, the sign of the thermopower alone is not always sufficient for a conclusion on the major mobile point defect and its concentration.

In Section 2.6 and Section 2.7 we calculated the thermopower of inhomogeneous electrolytes with defect concentration profiles corresponding to space charge regions. As shown by examples, these can be approximated by simple bicrystals representing the bulk and a homogeneous space charge layer with mean defect concentrations. Thus, one will not be able to decide whether a conductivity enhancement is due to the presence of extended space charge regions with increased defect concentrations but identical crystallographic properties or due to the presence of a second electrolyte phase with completely different crystallographic properties and a different defect

structure. This information can only be obtained from additional structural investigations.

A yet unresolved and theoretically complicated problem concerns the partial entropies $S_i^\circ(S_v^\circ)$ and heats of transport $Q_i^*(Q_v^*)$ of the individual lattice point defects in boundary regions. The present analysis is based on the assumption that both quantities are identical for the pure crystal and the composite. On subtracting the thermopower of the pure electrolyte from the composite electrolyte this assumption alone leads to the cancellation of the defect entropies and heats of transport and simplifies the foregoing analysis considerably. In the case of homogeneous doping this assumption is clearly justified, since the dopant itself occupies regular lattice sites and will – at least in a first order approximation – lead to only minor modifications of the spectrum of lattice vibrations. The presence of a ''heterogeneous'' dopant (the dispersed inert phase), however, introduces inner interfaces and will cause severe changes in the phonon spectrum of the electrolyte phase close to these interfaces. In addition, serious elastic distortions in the electrolyte can be induced by these interfaces, which may modify the defect thermodynamics. In the present treatment we neglect these effects.

A serious conductivity enhancement requires that $\alpha_{v,0}$ is high which is usually the case at relatively low temperatures. In the systems that have been investigated so far these low temperatures correspond to space charge regions with the Debye length extending to the micron scale. We can conclude that lattice vibrations with short wave lengths in the order a few Angstroms or nanometers within the space charge region will not be disturbed by the presence of the inert phase. Since the defect entropies S_i° and S_v° are mainly related to such lattice vibrations with short wave lengths, we can safely assume that the mean defect entropies in space charge regions are virtually independent of the presence of a second phase.

The situation is less clear for the defect heats of transport. So far no conclusive theoretical model for the microscopic interpretation of heats of transport is available. Recent theoretical calculations by Jones et al. [34–36] suggest that lattice vibrations with longer wave lengths contribute significantly to the heat of transport. Thus, the heat of transport of a point defect in a boundary region may be influenced more seriously by the presence of the boundary than the defect entropy. In the current state of understanding it appears nevertheless reasonable to assume constant defect heats of transport throughout the electrolyte phase. Even if the heats of transport were influenced by the presence of a second phase, this effect will most probably be of minor importance for the magnitude of the thermopower change on incorporating a second phase.

5. Conclusions

The results of the formal analysis show a close equivalence of results for homogeneous and heterogeneous doping in case of AgCl, which can be regarded as a model system. In particular, the temperature dependence of the thermopower is virtually identical. The explanation for this similarity is simple: The ionic thermopower of AgCl is governed by the local cation Frenkel equilibrium. Both homogeneous doping and heterogeneous doping (in terms of the space charge model) lead to a shift of this equilibrium. In the first case, a homogeneous solution of aliovalent cations shifts the intrinsic defect concentrations to different values. In the second case, a heterogeneous electrochemical (adsorption) equilibrium leads to the shift of the defect concentrations in locally restricted space charge regions. Thus, in both cases the average concentration of mobile defects is changed upon introduction of impurities. The different local distribution (homogeneous or inhomogeneous) of these additional defects is not detectable by an ionic thermopower measurement.

On the basis of the above arguments we conclude that the present formal treatment of the ionic thermopower of electrolyte composites is justified and provides a reasonable extension of the concept of space charge conduction by Maier [2]. Major assumptions so far concern the homogeneous temperature distribution and the simplifying geometric arguments. For a more precise formal treatment, an inhomogeneous temperature distribution and non-ideal geometries could be taken into account by finite element methods. Though the treatment is focused on ionic defects, all relations can be transferred

directly to electronic defects in Boltzmann-type semiconductors and composites of semiconductors containing extended space charge regions. Specific geometries can be represented by adequate networks of space charge regions parallel or perpendicular to temperature gradient.

6. List of symbols

Constants

e_0	electron charge
F	Faraday constant
k	Boltzmann constant
N_A	Avogadro's constant
R	universal gas constant
$\epsilon_{0,r}$	dielectric permeability

Chemical symbols

A	metal component
B	divalent metal component
X	non-metal component
S	divalent non-metal component
z_j	charge number of species j

Symbols for thermodynamic and kinetic quantities

$A=(Q_i^*-Q_v^*-\Delta H_F^\circ)/2$ $B=(Q_i^*-Q_v^*)/2$ $C=(S_i^\circ+S_v^\circ)/2$	short notation of parameters in Eq. (17)
c_j	molar concentration of species j
$c_i^\#$	concentration of interstitials in pure AX
$E_{a,\sigma}$	activation energy from conductivity experiments
H	molar enthalpy
$\Delta H_{m,def}$	migration enthalpy of defects
G	Gibbs free enthalpy
I	electric current
j_{A^+}	molar flux of component A
K_F	equilibrium constant of the Frenkel reaction
L_j	phenomenological transport coefficient of species j
Q_i^*,Q_v^*	reduced heat of transport of interstitials resp. vacancies
$R=\sigma\Delta z/A_{cr}$	Ohmic resistance
S_A°	molar standard entropy of metal A
S_i°,S_v°	standard entropy of interstitials resp. vacancies
$\bar{S}_{A^+}$	partial molar entropy of component A in AX
$S_{A^+}^*$	entropy of transport of component A in AX
T	absolute temperature
t_j	electric transference number of species j
u_i,u_v	electrochemical mobility of interstitials resp. vacancies
U	thermal emf
ΔU	difference between the emf of an inhomogeneous crystal resp. bicrystal and a pure crystal of the same size
V_m	molar volume of compound AX
x_j	molar fraction of compound j
$\alpha_i\equiv c_i/c_i^\#$	normalized concentration of interstitial defects
$\alpha(\tau)=(1-\vartheta_v\exp(-\tau))^2/(1+\vartheta_v\exp(-\tau))^2$	defect concentration profile in a space charge region
$\alpha_{v,0};\alpha_{i,0}$	concentration of vacancies resp. interstitials in the crystal layer next to the interface
$\epsilon\equiv d\varphi/dT$	thermoelectric power of a thermocell
ϵ_{A^+}	absolute cationic thermoelectric power as defined in Eq. (5)
$\Delta\epsilon$	difference between the thermopower of an inhomogeneous crystal resp. bicrystal and a pure crystal of the same size
φ	Galvani potential
$\psi_i\equiv u_i/u_v$	ratio of the mobilities of interstitials and vacancies
λ_D	Debye length
μ_j	chemical potential of the species j
$\tilde{\mu}_j=\mu_j+z_jF\varphi$	electrochemical potential of the species j
σ_{A^+}	ionic conductivity of cations A^+
$\vartheta_v=(\sqrt{\alpha_{v,0}}-1)/(\sqrt{\alpha_{v,0}}+1)$	dimensionless parameter describing the defect adsorption (Eq. (24))

Geometric quantities

A_{cr}	cross section of sample of compound AX

a_x,a_z	volume fraction of the doped part of a bicrystal
x,y,z	Cartesian coordinates
ξ,χ,ζ	normalized spatial coordinates
Δx,Δy,Δz	size of one part of a bicrystal in x, y or z-direction
$\Delta\xi$,$\Delta\chi$,$\Delta\zeta$	size of a crystal with an inhomogeneous concentration of defects
r_A	half length of a cubic dopant grain
V	volume
ϕ	volume fraction of heterogeneous dopant
ρ	normalized half length of a dopant grain

Subscripts

F	Frenkel defect formation
i	interstitial ion
q	heat
SA	surface interaction reaction
v	vacancy
$\perp$	perpendicular
$\parallel$	parallel
0	designates values in the crystal layer next to the interface
∞	designates values in the bulk of the crystal

Superscripts

I	designates (intrinsic) region of a bicrystal
II	designates homogeneously doped region of a bicrystal
I,II	designates properties of a bicrystal
$\circ$	designates standard values
#	designates pure (intrinsic) material

Acknowledgements

We are grateful to C. Korte for valuable comments and discussions. We thank H. Schmalzried, P. Heitjans, A.B. Lidiard and J. Maier for critical reading of the manuscript. This study is part of a project (DFG JA 648/3-1) funded by the DFG.

Appendix 1

Ionic thermopower in terms of lattice point defects

A complete derivation and description of the different transport properties of ions, electrons and components in the framework of linear irreversible thermodynamics can be found in [25] (see also [37]).

If we restrict ourselves to an ionic conductor $A_{\nu+\delta}X$ with Frenkel disorder in the cation sublattice and assume that the different defects do not interact ($L_{jk}=0$), two flux equations [17] are sufficient for the description of ionic transport:

$$j_\mathrm{i} = L_\mathrm{i}X_\mathrm{i} + L_{\mathrm{i}q}X_q = L_\mathrm{i}(X_\mathrm{i} + Q_\mathrm{i}^{*}X_q) \tag{54}$$

$$j_\mathrm{v} = L_\mathrm{v}X_\mathrm{v} + L_{\mathrm{v}q}X_q = L_\mathrm{v}(X_\mathrm{v} + Q_\mathrm{v}^{*}X_q) \tag{55}$$

with $Q_\mathrm{i}^{*} \equiv L_{\mathrm{i}q}/L_\mathrm{i}$ and $Q_\mathrm{v}^{*} \equiv L_{\mathrm{v}q}/L_\mathrm{v}$ defined as the so-called reduced heats of transport. The heat flux under isothermal conditions results as:

$$j_q = \sum_j Q_j^{*} \cdot j_j \quad (\nabla T = 0) \tag{56}$$

and with the reduced thermodynamic forces

$$X_j = -(\nabla\tilde{\mu}_j + \bar{S_j}\cdot\nabla T) \quad X_q = -\frac{1}{T}\cdot\nabla T \tag{57}$$

the cationic flux $j_{\mathrm{A}^+} \equiv j_\mathrm{i} - j_\mathrm{v}$ can be equated as:

$$j_{\mathrm{A}^+} = L_\mathrm{i}X_\mathrm{i} - L_\mathrm{v}X_\mathrm{v} + (L_\mathrm{i}Q_\mathrm{i}^{*} - L_\mathrm{v}Q_\mathrm{v}^{*})X_q \tag{58}$$

Due to the local Frenkel equilibrium only the two forces X_{A^+} and X_q remain as independent driving forces. The electrochemical potentials of the ions A^+ can be identified with the electrochemical potential of both building units:

$$\tilde{\mu}_{\mathrm{A}^+} = \tilde{\mu}_\mathrm{i} = -\tilde{\mu}_\mathrm{v} \tag{59}$$

Taking this local equilibrium into account, the forces X_j and X_q are related by:

$$X_{\mathrm{A}^+} + \bar{S}_{\mathrm{A}^+}\nabla T = X_\mathrm{i} + \bar{S}_\mathrm{i}\nabla T = -(X_\mathrm{v} + \bar{S}_\mathrm{v}\nabla T) \tag{60}$$

Inserting Eq. (60) into Eq. (58) we obtain

$$j_{\mathrm{A}^+} = -(L_\mathrm{i} + L_\mathrm{v}) \times \left[\nabla\tilde{\mu}_{\mathrm{A}^+} + \left(t_\mathrm{i}\bar{S}_\mathrm{i} - t_\mathrm{v}\bar{S}_\mathrm{v} + \frac{t_\mathrm{i}Q_\mathrm{i}^{*} - t_\mathrm{v}Q_\mathrm{v}^{*}}{T}\right)\nabla T\right] \tag{61}$$

with the electric transference numbers defined as $t_v \equiv L_v/(L_i + L_v)$ and $t_i \equiv L_i/(L_i + L_v)$. The thermopower of the ions follows from the condition $j_{A^+} = 0$ and with the definition in Eq. (5) as

$$\epsilon_{A^+} \equiv \frac{1}{F}\left(\frac{d\mu_{A^+}}{dT} + S^\circ_A\right)_{j_{A^+}=0} = -\frac{1}{F}\left(t_i\bar{S}_i - t_v\bar{S}_v + \frac{t_i Q^*_i - t_v Q^*_v}{T} - S^\circ_A\right) \tag{62}$$

Applying the equilibrium condition in Eq. (11), the definitions of the normalized defect concentrations α_i and α_v in Eq. (13), the mobility ratio $\psi_i = u_i/u_v$ and the relations

$$L_j = c_j u_j \tag{63}$$

and

$$\bar{S}_j = S^\circ_j - R\ln c_j \tag{64}$$

one obtains after some algebra the relation

$$\epsilon_{A^+} = -\frac{1}{F}\left[\frac{Q^*_i + Q^*_v + \Delta H^\circ_F}{2T}(t_i - t_v) - R\ln\alpha_i + \frac{Q^*_i - Q^*_v}{2T} + \frac{S^\circ_i - S^\circ_v}{2} - S^\circ_A\right] \tag{65}$$

Expressing the transference numbers by the normalized quantities ψ_i, and α_i, Eq. (65) can be written alternatively as

$$\epsilon_{A^+} = -\frac{1}{F}\left(\frac{Q^*_i + Q^*_v + \Delta H^\circ_F}{2T}\cdot\frac{\psi_i\alpha_i^2 - 1}{\psi_i\alpha_i^2 + 1} - R\ln\alpha_i + \frac{Q^*_i - Q^*_v}{2T} + \frac{S^\circ_i - S^\circ_v}{2} - S^\circ_A\right) \tag{66}$$

or

$$\epsilon_{A^+} = -\frac{1}{F}\left[\frac{Q^*_i + Q^*_v + \Delta H^\circ_F}{2T}\tanh(\ln\psi_i^{1/2}\alpha_i) - R\ln\alpha_i + \frac{Q^*_i - Q^*_v}{2T} + \frac{S^\circ_i - S^\circ_v}{2} - S^\circ_A\right] \tag{67}$$

Appendix 2

The non-isothermal space charge layer

For the calculation of the electric potential distribution in a space charge layer one has to solve the Poisson-Boltzmann equation. Starting point in case of an isothermal system is the electrochemical equilibrium within the space charge layer, expressed by the condition $\tilde{\mu}_j(\xi) = \mu_j(\xi) + z_j F\cdot\phi(\xi) = \tilde{\mu}_j(\xi_\infty)$. In the non-isothermal case we start with the flux equation for e.g. the interstitial defects as given by Eqs. (54) and (57) in Appendix (A.1). Under equilibrium conditions, this flux becomes zero and we obtain:

$$d\tilde{\mu}_i = d\mu_i + z_i F d\varphi = -\left(\bar{S}_i + \frac{Q^*_i}{T}\right)dT \tag{68}$$

As the chemical potential of the defects is a function of both concentration and temperature, i.e. $d\mu_i = RT\, d\ln c_i - S_i dT$ for an ideal system, Eq. (68) leads to:

$$d\ln c_i = -\left(\frac{z_i F}{RT}d\varphi + \frac{Q^*_i}{RT}\frac{dT}{T}\right) \tag{69}$$

For $dT = 0$ this equation reduces to the usual isothermal Boltzmann-type equation

$$\frac{c_i(\xi_0)}{c_i(\xi_\infty)} = \exp\left\{-\frac{z_i F}{RT}[\varphi(\xi_0) - \varphi(\xi_\infty)]\right\} \tag{70}$$

which relates the concentration ratio of charged species (ξ_0 denotes the position of the crystal layer next to the interface, ξ_∞ represents a position in the bulk outside the space charge region) to a compensating electric potential difference. For $dT \neq 0$ the exponential includes an additional term which represents the influence of the temperature gradient. Essentially, three thermodynamic forces are now involved which have to compensate in order to maintain thermodynamic equilibrium. For $dc_i = 0$, one obtains the usual expression

$$d\varphi = -\frac{1}{z_i F}\frac{Q^*_i}{T}dT \tag{71}$$

for the homogeneous thermovoltage of an intrinsic material.

Finally, a comparison of the different contributions of the three forces to Eq. (69) shows that the influence of the temperature difference on the force balance is negligible if not too small concentration ratios are involved. In the present case of space regions in solid electrolytes we assume in accordance with the results of Maier [2] that charged defect adsorption at an interface may lead to concentration ratios $c_i(\xi_0)/c_i(\xi_\infty)$ of counter-charged defects of several orders of magnitude, i.e. $\ln[c_i(\xi_0)/c_i(\xi_\infty)]$ is in the order of 10^1. In fact, only adsorption effects of such magnitude will cause detectable excess conductivities (thermopower). Regarding now the integrated Eq. (69) with a mean temperature $\bar{T}$,

$$\underbrace{\ln\frac{c_i(\xi_0)}{c_i(\xi_\infty)}}_{\cong 10^1} = -\left\{\underbrace{\frac{z_i F}{R\bar{T}}\left[\varphi(\xi_0)-\varphi(\xi_\infty)\right]}_{\cong 10^1} + \underbrace{\frac{Q_i^*}{R\bar{T}}\frac{T(\xi=\infty)-T(\xi_0)}{\bar{T}}}_{\cong 10^{-6}}\right\} \tag{72}$$

we realize that the temperature gradient term[3] is typically only of the order of 10^{-6}, with $Q_i^*/\mathrm{RT}\cong 1$ and $\Delta T/T\cong 10^{-6}$. Thus, a small temperature difference which is applied in a typical thermopower experiment will not cause any detectable change of the defect concentrations in the space charge region. The reason of this minor influence is given by the fact that typical ''chemical'' reaction enthalpies (here for a specific adsorption equilibrium) are by far larger than the small thermal energy differences caused by ΔT. The use of an isothermal solution of the Poisson-Boltzmann equation for the calculation of the thermopower of space charge regions is thus justified.

[3]With an experimental temperature gradient of 10 K/cm and an estimated Debye length of 0.1 μm at $T=400$K, the normalized temperature difference across a single space charge layer becomes $\Delta T/T\simeq 2.5\cdot 10^{-7}$.

Appendix 3

Integration of the concentration profile for the perpendicular case

Expressing the hyperbolic functions in Eq. (46) by exponential functions one obtains:

$$\Delta\epsilon_{A^+,\perp} = -\frac{1}{F\Delta\zeta}\cdot\left\{\frac{A}{T}\cdot\int_0^{\Delta\zeta}\frac{\psi_i[\alpha_i(\zeta)]^2-1}{\psi_i[\alpha_i(\zeta)]^2+1}-\frac{\psi_i-1}{\psi_i+1}\,d\zeta - R\int_0^{\Delta\zeta}\ln\alpha_i(\zeta)d\zeta\right\} \tag{73}$$

which can be transformed by some algebra to the following sum of three integrals

$$\Delta\varepsilon_{A^+,\perp} = -\frac{1}{F\Delta\zeta}\cdot\left[\frac{A}{T}\cdot\frac{2}{\psi_i+1}\left\{\underbrace{\int_0^{\Delta\zeta}d\zeta}_{I_1} - \underbrace{\int_0^{\Delta\zeta}\frac{\psi_i+1}{\psi_i[\alpha_i(\zeta)]^2+1}d\zeta}_{I_2}\right\} - R\underbrace{\int_0^{\Delta\zeta}\ln\alpha_i(\zeta)d\zeta}_{I_3}\right] \tag{74}$$

The first integral I_1 is simply $\int_0^{\Delta\zeta}d\zeta=\Delta\zeta$. Inserting the concentration function from Eq. (22) the second integral I_2 reads

$$\int_0^{\Delta\zeta}\frac{\psi_i+1}{\psi_i[1-e^{-\zeta}\vartheta_v]^4[1+e^{-\zeta}\vartheta_v]^{-4}+1}\,d\zeta. \tag{75}$$

I_2 can be solved applying the substitution $\gamma_1=\frac{1}{2}(\ln\vartheta_v-\zeta)$:

$$\int_{1/2\ln\vartheta_v}^{1/2(\ln\vartheta_v-\Delta\zeta)}\frac{-2(\psi_i+1)}{\psi_i\tanh^4(\gamma_1)+1}\,d\gamma_1 = \frac{1}{2\sqrt{2}}(\psi_i^{3/4} - \psi_i^{1/4})\ln\left[\frac{1-\sqrt{2}\psi_i^{1/4}\tanh(\gamma_1)+\sqrt{\psi_i}\tanh^2(\gamma_1)}{1+\sqrt{2}\psi_i^{1/4}\tanh(\gamma_1)+\sqrt{\psi_i}\tanh^2(\gamma_1)}\right] + \frac{1}{\sqrt{2}}(\psi_i^{3/4}+\psi_i^{1/4})\{\arctan[1-\sqrt{2}\psi_i^{1/4}\tanh(\gamma_1)]$$

$$- \arctan[1 + \sqrt{2}\psi_i^{1/4} \tanh(\gamma_1)]\} - 2\gamma_1\Big|_{1/2 \ln \vartheta_v}^{1/2(\ln \vartheta_v - \Delta\zeta)} \tag{76}$$

The integral I_3

$$\int_0^{\Delta\zeta} \ln \frac{[1 - e^{-\zeta}\vartheta_v]^2}{[1 + e^{-\zeta}\vartheta_v]^2} \, d\zeta = 2 \int_0^{\Delta\zeta} \ln[1 - e^{-\zeta}\vartheta_v] d\zeta - 2 \int_0^{\Delta\zeta} \ln[1 + e^{-\zeta}\vartheta_v] d\zeta \tag{77}$$

can be solved by substituting the numerator integral of Eq. (77) with $\gamma_2 = 1 - e^{-\zeta}\vartheta_v$ and the denominator integral with $\gamma_3 = 1 + e^{-\zeta}\vartheta_v$ resulting in

$$2 \int_{1-\vartheta_v}^{1-e^{-\Delta\zeta}\vartheta_v} \frac{\ln \gamma_2}{1 - \gamma_2} \, d\zeta - 2 \int_{1+\vartheta_v}^{1+e^{-\Delta\zeta}\vartheta_v} \frac{\ln \gamma_3}{1 - \gamma_3} \, d\zeta \tag{78}$$

$$= 2[\text{dilog}(1 - e^{-\Delta\zeta}\vartheta_v) - \text{dilog}(1 - \vartheta_v) - \text{dilog}(1 + e^{-\Delta\zeta}\vartheta_v) + \text{dilog}(1 + \vartheta_v)], \tag{79}$$

with the dilogarithm function defined as $\text{dilog}(x) \equiv -\int_1^x \ln(\tau)/(\tau - 1) d\tau$.

Appendix 4

Integration of the concentration profile for the parallel case

The solution of Eq. (49) is divided into two parts. The integral in the numerator including the product of the transport coefficient and the entropy of transport is solved firstly.

Transferring the numerator in Eq. (49) to exponential functions leads to

$$-\frac{1}{F} \cdot \left[\int_0^{\Delta\xi} [\psi_i \alpha_i(\xi) + \alpha_i(\xi)^{-1}] \cdot \left[\frac{A}{T} \frac{2}{\psi_i + 1} \left\{ 1 - \frac{\psi_i + 1}{\psi_i \alpha_i(\xi)^2 + 1} \right\} - R \ln \alpha_i(\xi) \right] d\xi \right] \tag{80}$$

Regrouping the terms in Eq. (80) one gets

$$-\frac{1}{F} \cdot \left[\frac{A}{T} \frac{2\psi_i}{\psi_i + 1} \left\{ \underbrace{\int_0^{\Delta\xi} \alpha_i(\xi) d\xi}_{I_4} - \underbrace{\int_0^{\Delta\xi} \frac{1}{\alpha_i(\xi)} d\xi}_{I_5} \right\} - R \left\{ \psi_i \underbrace{\int_0^{\Delta\xi} \alpha_i(\xi) \cdot \ln \alpha_i(\xi) d\xi}_{I_6} + \underbrace{\int_0^{\Delta\xi} \frac{\ln \alpha_i(\xi)}{\alpha_i(\xi)} d\xi}_{I_7} \right\} \right] \tag{81}$$

After insertion of the concentration profile of defects (Eq. (22)), the integrals I_4 and I_5 are solved by the substitutions γ_3 resp. γ_2 as used in Eq. (78) (cf. [29]):

$$\int_0^{\Delta\xi} \frac{[1 - \vartheta_v \cdot \exp(-\xi)]^2}{[1 + \vartheta_v \cdot \exp(-\xi)]^2} \, d\xi = \frac{4}{1 + \vartheta_v} - \frac{4}{1 + \vartheta_v \exp(-\Delta\xi)} + \Delta\xi \tag{82}$$

$$\int_0^{\Delta\xi} \frac{[1 + \vartheta_v \cdot \exp(-\xi)]^2}{[1 - \vartheta_v \cdot \exp(-\xi)]^2} \, d\xi = \frac{4}{1 - \vartheta_v} - \frac{4}{1 - \vartheta_v \exp(-\Delta\xi)} + \Delta\xi \tag{83}$$

The integral I_6 is solved by the substitution γ_3 leading to

$$\int_{1+\vartheta_v}^{1+\vartheta_v \exp(-\Delta\xi)} -\frac{(2 - \gamma_3)^2}{\gamma_3^2(\gamma_3 - 1)} \ln \left[\frac{(2 - \gamma_3)^2}{\gamma_3^2} \right] d\gamma_3 = \tag{84}$$

$$2 \int_{1+\vartheta_v}^{1+\vartheta_v \exp(-\Delta\xi)} \frac{4 \ln(2 - \gamma_3)}{\gamma_3^2} - \frac{4 \ln(\gamma_3)}{\gamma_3^2} - \frac{\ln(2 - \gamma_3)}{\gamma_3 - 1} + \frac{\ln(\gamma_3)}{\gamma_3 - 1} d\gamma_3 = \tag{85}$$

$$4 \ln \left[2 \frac{(2 - \gamma_3)}{\gamma_3} \right] + \frac{8}{\gamma_3} \left\{ 1 + \ln \left[\frac{\gamma_3}{2 - \gamma_3} \right] \right\} - 2 \, \text{dilog}(\gamma_3) + 2 \, \text{dilog}(2 - \gamma_3) \Big|_{1+\vartheta_v}^{1+\vartheta_v \exp(-\Delta\xi)} \tag{86}$$

Applying the substitution of γ_2 to the integral I_7 leads to a similar integral as in Eq. (84) which results as:

$$\int_{1-\vartheta_v}^{1-\vartheta_v \exp(-\Delta\xi)} -\frac{(2-\gamma_3)^2}{\gamma_3^2(\gamma_3-1)} \ln\left[\frac{(2-\gamma_3)^2}{\gamma_3^2}\right] d\gamma_3 = \tag{87}$$

$$4 \ln\left[2\frac{(2-\gamma_2)}{\gamma_2}\right] + \frac{8}{\gamma_2}\left\{1 + \ln\left[\frac{\gamma_2}{2-\gamma_2}\right]\right\} - 2\,\mathrm{dilog}(\gamma_2) + 2\,\mathrm{dilog}(2-\gamma_2)\Big|_{1-\vartheta_v}^{1-\vartheta_v \exp(-\Delta\xi)} \tag{88}$$

The denominator is given by already solved integrals (Eqs. (82) and (83)):

$$\psi_i \int_0^{\Delta\xi} \underbrace{\alpha_i(\xi)}_{I_4} d\xi + \int_0^{\Delta\xi} \underbrace{\alpha_i(\xi)^{-1}}_{I_5} d\xi \tag{89}$$

Finally, the thermopower difference is given by the quotient of Eq. (81) and Eq. (89).

References

[1] C.C. Liang, J. Electrochem. Soc. 120 (1973) 1289–1292.
[2] J. Maier, Prog. Solid State Chem. 23 (1995) 171–263.
[3] J.B. Wagner, in: T. Takahashi (Ed.), High Conductivity Conductors Solid Ionic Conductors. World Scientific, Singapore, 1989, pp. 146–165.
[4] N.J. Dudney, Ann. Rev. Mat. Sci. 19 (1989) 103–120.
[5] J. Frenkel, Kinetic Theory of Liquids. Oxford University Press, Oxford, 1946.
[6] K. Lehovec, J. Chem Phys. 21(7) (1953) 1123–1128.
[7] K.L. Kliewer, J.S. Koehler, Phys. Rev. A 140(4) (1965) 1226–1247.
[8] K.L. Kliewer, J. Phys. Chem. Solids 27 (1966) 705–725.
[9] K. Seeger, Semiconductor Physics, 5th ed. Springer Verlag, Berlin, 1991.
[10] G.H. Jonker, Philips Res. Repts. 23 (1968) 131–138.
[11] R.W. Christy, J. Chem. Phys. 34 (1961) 1148–1155.
[12] A.B. Lidiard, Handbuch der Physik, Vol. XX, Electrical Conductivity II, Ionic Conductivity. Springer Verlag, Berlin, 1957, pp. 246–349.
[13] R.E. Howard, A.B. Lidiard, Phil. Mag. 2 (1957) 1462.
[14] K. Shahi, J.B. Wagner, J. Electrochem. Soc. 128(1) (1981) 6–13.
[15] C. Wagner, Prog. Solid State Chem. 7 (1972) 1–37.
[16] I. Prigogine, Introduction to Thermodynamics of Irreversible Processes. Interscience Publishers, New York, London, 1955.
[17] A.R. Allnatt, A.B. Lidiard, Atomic Transport in Solids. Cambridge University Press, Cambridge, 1993.
[18] J. Teltow, Ann. Phys. 6 (1949) 63–71.
[19] J. Janek, C. Korte, Solid State Ionics 92 (1996) 193–204.
[20] E. Haga, J. Phys. Soc. Jap., 13(10) (1958) 1090; 14(8) (1959) 992; 14(9) (1959) 1176; 15(11) (1960) 1949.
[21] J. Tauc, Czechosl. J. Phys. 3 (1953) 4.
[22] V.A. Johnson, K. Lark-Horovitz, Phys. Rev. 26 (1953) 226.
[23] G. Lantz, Z. Naturforschg. 8a (1953) 361–371.
[24] J.H. Becker, H.P.R. Frederikse, J. Appl. Phys., Suppl. 23(1) (1962) 447–453.
[25] C. Korte, Nichtisotherme Transportprozesse in gemischtleitenden Ionenkristallen. Ph.D. thesis, Universität Hannover, 1996.
[26] C. Korte, J. Janek, Z. Phys. Chem. Solids 206 (1998) 129–163.
[27] H.I. Yoo, D.-S. Sinn, J.-O. Hong, J. Electrochem. Soc. 145(3) (1997) 1008–1016.
[28] J. Maier, Phys. Chem. Solids 46(3) (1985) 309–320.
[29] J. Maier, Ber. Bunsenges. Phys. Chem. 90 (1986) 26–33.
[30] J.-S. Lee, J. Maier, Electrochem. Soc. Proc. 97(24) (1998) 751–763.
[31] J. Maier, private communication.
[32] M. Vennekamp, Transporteigenschaften von heterogen dotierten Ionenleitern. Diploma thesis, Universität Hannover, 1997.
[33] C. Korte, J. Janek, J. Phys. Chem. Solids 58(4) (1997) 623–637.
[34] C. Jones, P.J. Grout, A.B. Lidiard, Phil. Mag. Lett. 74 (1996) 217.
[35] C. Jones, P.J. Grout, A.B. Lidiard, Ber. Bunsenges. Phys. Chem. 101(9) (1997) 1232–1237.
[36] C. Jones, Heats of Transport in Defective Solids. D. Phil. thesis, University of Oxford, Oxford, 1997.
[37] J. Janek, C. Korte, Z. Phys. Chem. 196 (1996) 187–208.